

# Geochronology of northern Hogem batholith, Quesnel terrane, north-central British Columbia



Jones, G.<sup>1,2</sup>, Ootes, L.<sup>1,a</sup>, Milidragovic, D.<sup>1,3</sup>, Friedman, R.<sup>4</sup>, Camacho, A.<sup>5</sup>, Luo, Y.<sup>2</sup>, Vezinet, A.<sup>2</sup>, Pearson, D.G.<sup>2</sup>, and Schiarizza, P.<sup>1</sup>

<sup>1</sup>British Columbia Geological Survey, Ministry of Energy, Mines and Low Carbon Innovation, Victoria, BC, V8W 9N3

<sup>2</sup>Department of Earth & Atmospheric Sciences, University of Alberta, Edmonton, AB, T6G 2E3

<sup>3</sup>Geological Survey of Canada, Natural Resources Canada, Vancouver, BC, V6B 5J3

<sup>4</sup>Pacific Centre for Geochemical and Isotopic Research, University of British Columbia, Vancouver, BC, V6T 1Z4

<sup>5</sup>Department of Geological Sciences, University of Manitoba, Winnipeg, MB R3T 2N2

<sup>a</sup>corresponding author: Luke.Ootes@gov.bc.ca

Recommended citation: Jones, G., Ootes, L., Milidragovic, D., Friedman, R., Camacho, A., Luo, Y., Vezinet, A., Pearson, D.G., and Schiarizza, P., 2021. Geochronology of northern Hogem batholith, Quesnel terrane, north-central British Columbia. In: Geological Fieldwork 2020, British Columbia Ministry of Energy, Mines and Low Carbon Innovation, British Columbia Geological Survey Paper 2021-01, pp. 37-56.

## Abstract

New and previously unpublished geochronological data that complement bedrock mapping and geochemical studies in northern Hogem batholith indicate punctuated emplacement of four distinct intrusive suites during a protracted (ca. 80 Ma) interval, from 207 to 128 Ma. U-Pb crystallization ages include new zircon (by LA-ICP-MS), previously unpublished legacy zircon and titanite (by ID-TIMS), and published zircon (by CA-TIMS). Amphibole, biotite, and muscovite <sup>40</sup>Ar/<sup>39</sup>Ar step-heating results provide magmatic cooling ages and post-deformation cooling ages. The Thane Creek suite, composed of mostly metaluminous diorite to quartz monzodiorite with lesser hornblende, intruded host Nicola Group strata between 207 and 194 Ma. The Duckling Creek suite consists of alkaline biotite clinopyroxene and syenite that intruded the Thane Creek suite between 182 and 175 Ma. The Osilinka suite, represented by a weakly peraluminous leucocratic granite body, yielded a maximum emplacement age of ca. 160 Ma. The Mesilinka suite consists of metaluminous tonalite and weakly peraluminous granodiorite to granite, with interpreted crystallization ages ranging from 135 to 128 Ma. Bedrock mapping and geochronologic results from this study indicate that northern Hogem batholith contains prospective rocks comparable to those that host the Lorraine and other deposits south of the present study area. The Hogem batholith is relatively unique in the Canadian Cordillera because it contains a remarkable evolution of punctuated Upper Triassic to Lower Cretaceous intrusive suites that are compositionally and chemically diverse. A new discovery is that the Mesilinka suite (Lower Cretaceous) intruded during a Cordilleran-wide magmatic lull.

**Keywords:** Hogem batholith, Quesnel terrane, Stikine terrane, geochemistry, U-Pb zircon crystallization ages, CA-TIMS, ID-TIMS, LA-ICP-MS

## 1. Introduction

In 2018, the British Columbia Geological Survey initiated a three-year mapping project in the Omineca Mountains of north-central British Columbia (Figs. 1, 2; Ootes et al., 2019, 2020a-c). The project aims to better understand the bedrock and surficial geology and associated base- and precious-metal mineralization in the northern part of Hogem batholith and surroundings, through detailed 1:50,000-scale mapping and geochemical studies (Fig. 2; Ootes et al., 2020a). Herein we summarize the results of new U-Pb zircon, legacy U-Pb zircon and titanite, and <sup>40</sup>Ar/<sup>39</sup>Ar biotite, hornblende, and muscovite geochronology for northern Hogem batholith. Full details, including locations, data tables, zircon descriptions, and cathodoluminescence (CL) imagery are presented in Ootes et al. (2020c).

## 2. Geologic setting and previous work

### 2.1. Geology

In Quesnel terrane, Hogem batholith is bounded to the north

and east by volcanic and sedimentary rocks of the Nicola Group (Triassic) along fault and intrusive contacts (Fig. 1). To the west, the batholith and Nicola Group are juxtaposed against Cache Creek and Stikine terranes across the Pinchi-Ingenika dextral strike-slip fault system (Figs. 1, 2).

Hogem batholith is subdivided into four petrologically distinct intrusive units; from oldest to youngest these are the Thane Creek, Duckling Creek, Osilinka, and Mesilinka suites (Figs. 3, 4; Woodsworth, 1976; Schiarizza and Tan, 2005a, b; Devine et al., 2014; Ootes et al., 2019, 2020a-c). Full unit descriptions can be found in Ootes et al. (2019) and supporting geochemical data are in Ootes et al. (2020c). The intrusive suites span a range of compositions from ultramafic to highly silicic (SiO<sub>2</sub>=34.3-77.0 wt.%, on LOI-free anhydrous basis; Figs. 3, 4). In general, the metaluminous (Fig. 4) Thane Creek suite contains relatively small pockets (<0.01 km<sup>2</sup>) of coarse-grained hornblende that was intruded and co-mingled with medium-grained diorite to quartz monzodiorite (Fig. 3). The suite ranges from undeformed to strongly deformed, including

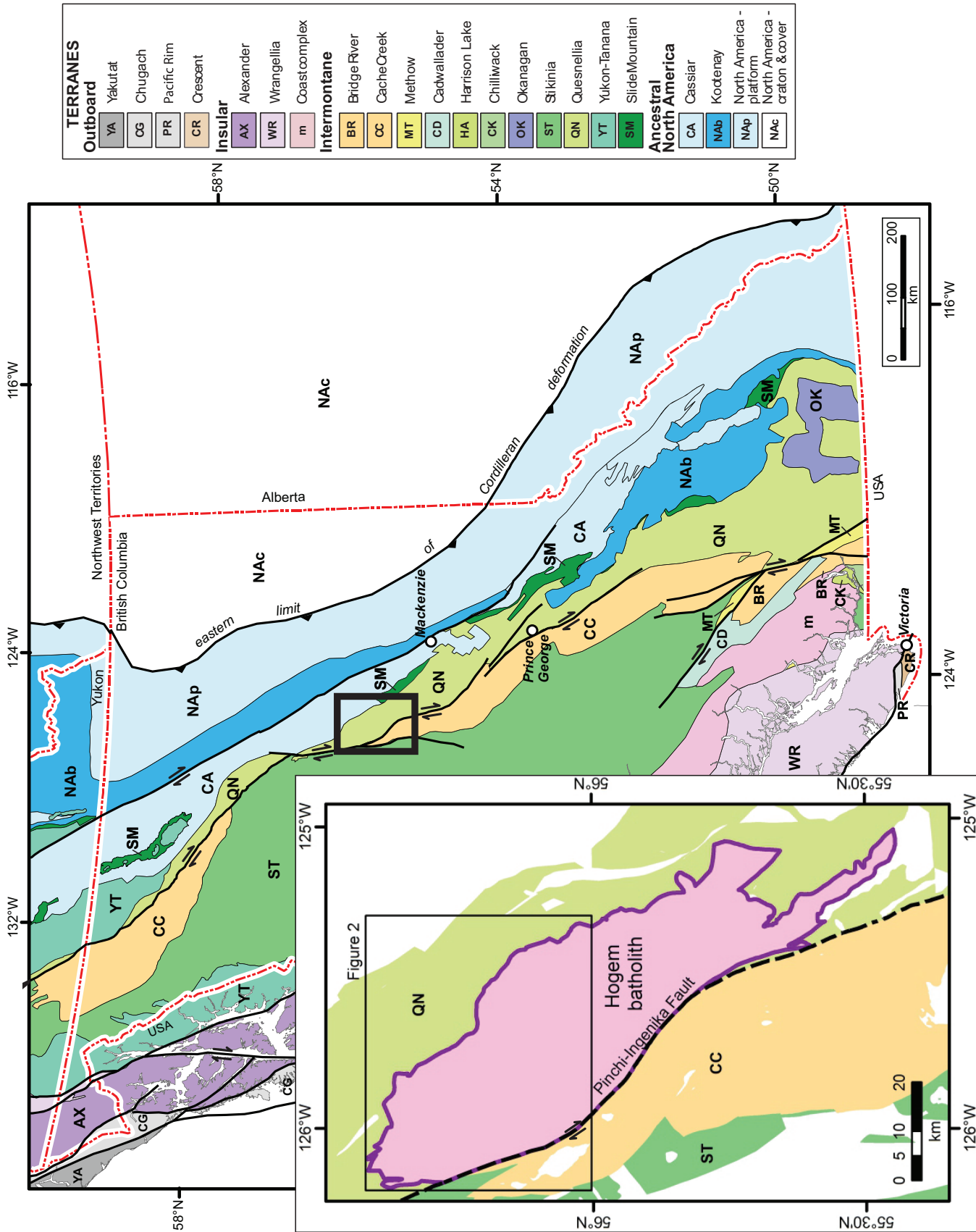


Fig. 1. Terrane map of British Columbia. Modified after Nelson et al. (2013). Inset map shows the Hogen batholith within Quesnell terrane.

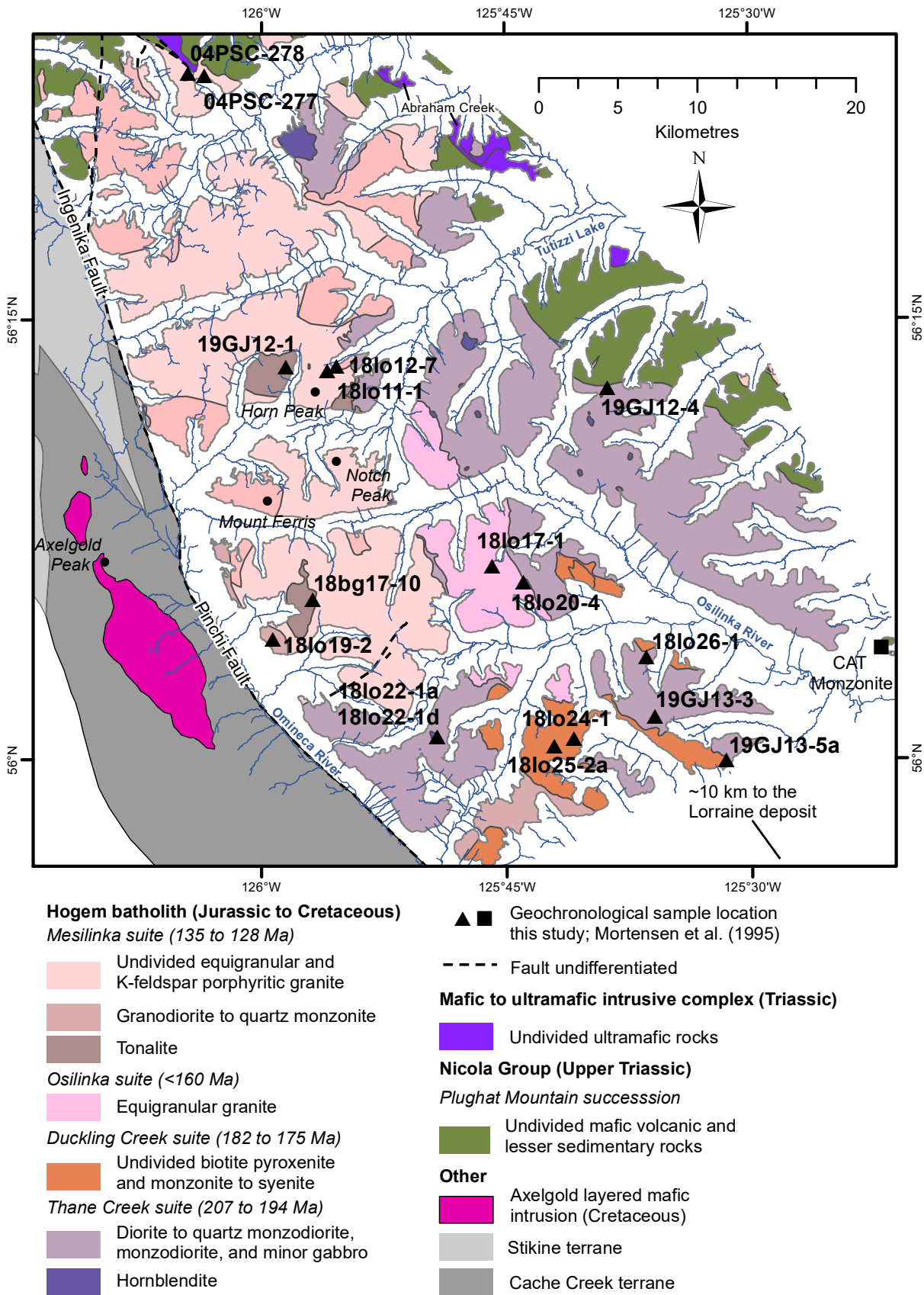
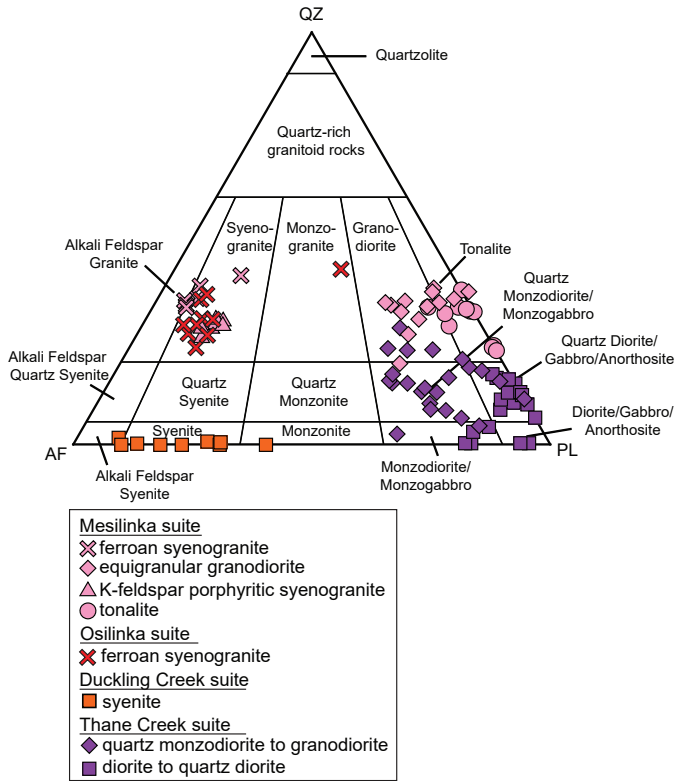


Fig. 2. Geology of northern Hogem batholith and its surroundings. The Hogem batholith is in the Quesnel terrane, which is separated from the Cache Creek and Stikine terranes by the Pinchi-Ingenika fault (dextral strike-slip). Modified after Ootes et al. (2020a).



**Fig. 3.** Quartz-alkali feldspar-plagioclase (QAP) diagram for classification of felsic igneous rocks (Le Maitre et al., 2002). Whole-rock geochemical compositions of samples from the Hogen batholith were converted to volumetric modal mineralogy using the methodology of Stanley (2017). Felsic samples from the Duckling Creek suite are mildly silica-undersaturated and plot on the feldspathoid side (not shown) of the alkali feldspar-plagioclase join.

local zones of mylonite. The Duckling Creek suite includes older biotite clinopyroxenite that is intruded by two-feldspar-bearing syenite, commonly with K-feldspar phenocrysts and local magmatic layering. In the north, the suite is weakly deformed (Ootes et al., 2019, 2020a, b), whereas in the Lorraine area to the south it is moderately to strongly deformed (e.g., Devine et al., 2014). Duckling Creek rocks are metaluminous and mildly silica undersaturated; the more felsic samples plot on the feldspathoid side of the QAP diagram (Fig. 3). Based on lower  $Al_2O_3$  and higher CaO at given  $SiO_2$ , the ultramafic rocks of the Duckling Creek suite are readily distinguished from the Thane Creek suite hornblendites (Fig. 4).

The Osilinka suite is a leucocratic medium-grained equigranular granite (Fig. 3), typically with less than 5% mafic minerals. The Osilinka suite is weakly peraluminous (Fig. 4). The intrusive rocks are deformed and although fabric development is cryptic in the granitic rocks, mafic dikes in the Osilinka suite locally contain shear fabrics (Ootes et al., 2019).

The Mesilinka suite contains at least four intrusive phases. The oldest (tonalite and granodiorite) are intruded by equigranular granite and K-feldspar porphyritic granite (Fig. 3). The suite ranges from weakly metaluminous (tonalites) to peraluminous

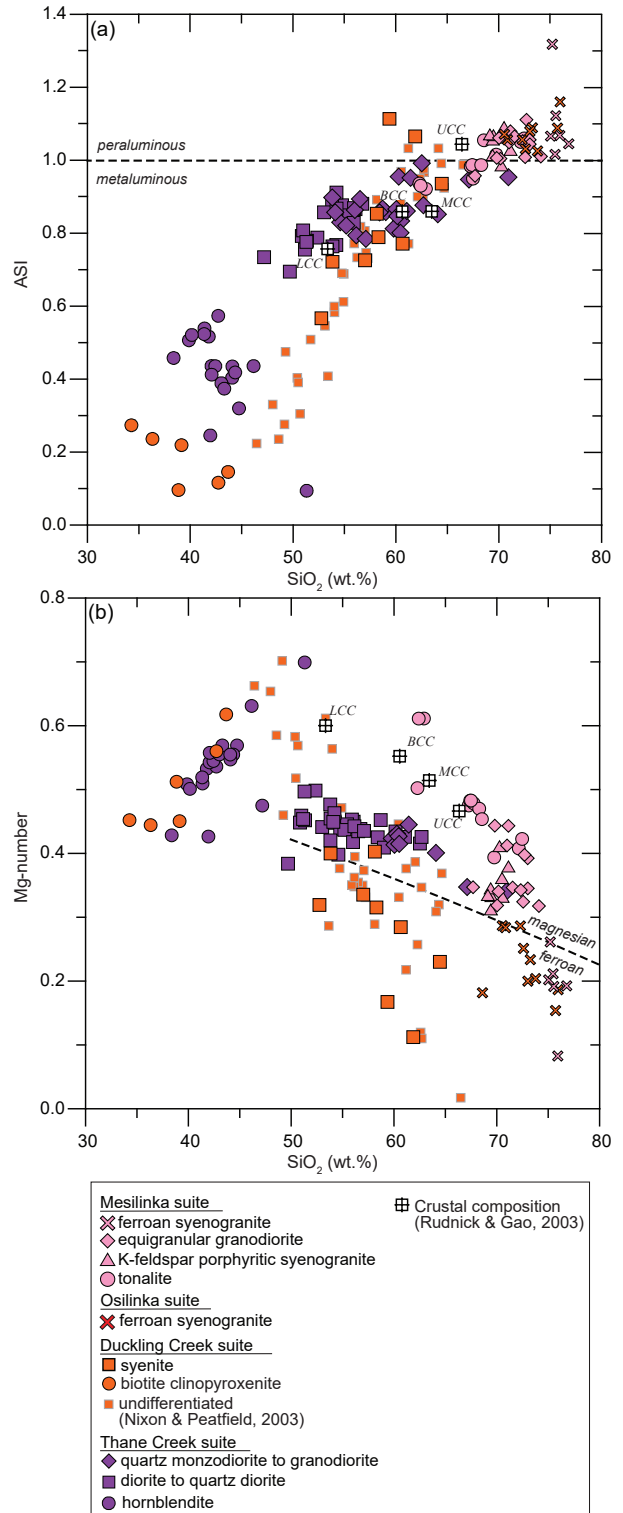


**Fig. 4.** Geochemical classification of plutonic suites of the Hogen batholith, including previously published analyses of Duckling Creek suite (Nixon and Peatfield, 2003). **a)** Aluminum saturation index ( $ASI = \text{molar } Al_2O_3 / (\text{CaO} - 1.67 P_2O_5 + Na_2O + K_2O)$ ; Shand, 1943) vs.  $SiO_2$  (wt.%). **b)** Mg-number (molar  $MgO / (MgO + FeO^{TOT})$ ) vs.  $SiO_2$  (wt.%). Magnesian and ferroan intermediate to felsic rocks are separated by the dashed line from Frost and Frost (2008). Shown for reference are the estimated compositions of lower (LCC), middle (MCC), upper (UCC) and bulk (BCC) continental crust (Rudnick and Gao, 2003).

(granite to granodiorite; Fig. 4). All the intrusive phases in the Mesilinka suite have a tectonic foliation that is defined by aligned biotite (Ootes et al., 2019, 2020a, b).

## 2.2. Previous work

Northern Hogem batholith (north of 56°N) was mapped by Armstrong (1946), Lord (1948, 1949), Armstrong and Roots (1948, 1954), Roots (1954), Irvine (1976), and Woodsworth (1976). Mapping by Ferri et al. (2001a, b), in areas to the east and northeast, focussed on the Takla Group in Quesnel terrane (referred to as the Nicola Group in this study; see discussion in Ootes et al., 2020b) and left Hogem batholith largely undivided. Schiarizza and Tan (2005a, b) mapped north of the study area and reported preliminary isotopic ages for plutonic rocks at the northern tip of Hogem batholith. Southern Hogem batholith (south of 56°N) was mapped and subdivided by Garnett (1972, 1978). Bath et al. (2014) and Devine et al. (2014) studied the Lorraine porphyry Cu-Au deposit southeast of the study area, providing isotopic ages for mineralization and host rocks. Nixon and Peatfield (2003) described rock types and presented geochemical data from the Lorraine deposit area. CGG Canada Services Ltd. (2018) presented the results of an airborne geophysical survey extending across much of the study area that includes both radiometric (K, U, Th) and magnetic data.

## 3. Methods

### 3.1. U-Pb geochronology

Samples collected in 2018 and 2019 were analyzed using laser ablation-inductively coupled plasma-mass spectrometry (LA-ICP-MS); samples collected in 2004 were analyzed using thermal ionization mass spectrometer (ID-TIMS). Table 1 summarizes the samples analyzed and preliminary results; the full analytical techniques and supporting data are in Ootes et al. (2020c).

#### 3.1.1. LA-ICP-MS

We collected unaltered rock samples weighing 5-10 kg for geochronology. Sample preparation and analysis were completed at the Canadian Centre for Isotopic Microanalysis (CCIM), University of Alberta. Approximately 1-2 kg of sample was cut, then disaggregated using the SELFRAG laboratory electronic pulse disaggregation system to yield high-quality mineral separates. Zircon separates were set in epoxy mounts and polished to expose grain mid-sections. Back-scattered electron (BSE), cathodoluminescence (CL), and secondary electron (SE) images of the zircon crystals (see Ootes et al., 2020c) were obtained using a Zeiss EVO MA15 scanning electron microscope at CCIM. These images were used to select spots for laser ablation U-Pb isotope analysis.

Zircon U-Pb isotope data were collected using laser ablation-inductively coupled plasma-mass spectrometry (LA-ICP-MS) with a RESolution 193 nm ArF excimer laser, equipped with a 2-volume Laurin-Technic S-155 ablation cell, and a Thermo Scientific Element-XR mass spectrometer. A subset of the zircon U-Pb data were collected using the laser ablation split-

stream (LASS)-ICP-MS method (e.g., Fisher et al., 2014) to simultaneously analyze U-Pb and Lu-Hf (Jones et al., 2021). All LA-ICP-MS data were reduced using Iolite software (Paton et al., 2010; Paton et al., 2011; Fisher et al., 2017). Trace element concentrations of most zircon crystals were determined during a separate analytical run in single stream or in LASS mode along with Lu-Hf (Jones et al., 2021). Not all zircon was analyzed for trace elements because of zircon grain size limitations.

After reduction, the data were filtered using trace element concentrations. Zircons with concentrations of Ca >300 ppm, Fe >300 ppm, Ti >20 ppm, and La >1 ppm were not considered in age calculations, because they may contain altered domains, or domains with mineral inclusions, which will affect the interpreted age of the sample. Zircon grains with significant common Pb were also filtered by rejecting data with  $f^{206}\text{Pb}_c$  values >1% (e.g., Vezinet et al., 2018; Ootes et al., 2020c). Zircon grains with >10% discordance, determined using the  $^{206}\text{Pb}/^{238}\text{U}$  and  $^{207}\text{Pb}/^{235}\text{U}$  ages, were also rejected. In addition to filtering the U-Pb data, the internal structures of zircon were examined using CL and BSE images. Xenocrystic or antecrystic cores were identified by the degree of roundness and crosscutting growth zones, and these grains were not used in calculating sample ages. After data filtering, individual zircon  $^{206}\text{Pb}/^{238}\text{U}$  ages were used to calculate a weighted mean  $^{206}\text{Pb}/^{238}\text{U}$  age for each sample using IsoplotR (Vermeesch, 2018). All U-Pb data are reported at the  $2\sigma$  (95.5%) confidence level.

Several samples yielded a spread in the  $^{206}\text{Pb}/^{238}\text{U}$  age data that is higher than a statistically reasonable mean squared weighted deviation (MSWD) of the weighted mean. Zircon in these samples were interpreted to be of the sample population, having passed the data reduction and filtering methods outlined above, so the spread in the zircon data was attributed to natural isotopic variation between crystals (geological scatter; Vermeesch, 2018). To reduce the spread in the data and lower the MSWD, an excess scatter constant (over-dispersion) was determined for each sample and added to the standard error of the individual analyses (Vermeesch, 2018; see sample 18lo25-2a (section 4.2.1.) for an example of filtering method results). After using excess scatter, the weighted mean  $^{206}\text{Pb}/^{238}\text{U}$  dates overlapped the concordia and non-processed weighted mean  $^{206}\text{Pb}/^{238}\text{U}$  dates, but with a reasonable MSWD. The robustness of these weighted mean  $^{206}\text{Pb}/^{238}\text{U}$  dates is shown by arbitrarily rejecting the youngest and oldest zircon dates in the sample to lower the MSWD, which yields a weighted mean  $^{206}\text{Pb}/^{238}\text{U}$  age that overlaps with the excessive scatter weighted mean  $^{206}\text{Pb}/^{238}\text{U}$  age (e.g., see sample 18lo25-2a, Fig. 7e, section 4.2.1.).

#### 3.1.2. Legacy ID-TIMS

Samples collected in 2004 were processed and analyzed soon thereafter at the Pacific Centre for Isotopic and Geochemical Research (PCIGR) at the University of British Columbia. Zircon and titanite were separated from samples

Table 1. Summary of samples and geochronological results.

Suite	Sample#	Rock type	Lat	Long	Geochronological result				Source	
					U-Pb (Ma)	Ar-Ar (Ma)	LA-ICPMS z <sup>a</sup>	hbl		
Mesiinka	04PSC-277	equigranular granite	56.3892	-126.0589						1
Mesiinka	04PSC-278	porphyritic granite	56.3905	-126.0757						1
Mesiinka	18o11-1	equigranular granite	56.221037	-125.932380			127.9±0.8			1
Mesiinka	18o12-7	porphyritic granite	56.223797	-125.923148			134.8±1.2			1
Mesiinka	19GJ12-1	tonalite	56.223775	-125.974787			134.1±0.5			1
Mesiinka	18BG17-10	tonalite	56.091248	-125.947834						1
Mesiinka	18BG17-10	tonalite	56.091248	-125.947834						1
Mesiinka	18o19-2	granodiorite	56.068745	-125.988290						1
Osiinka sheet	18o20-4	felsic porphyry	56.100984	-125.732593			162.2±2.6			1
Osiinka	18o17-1	granite	56.110442	-125.764089			159.2±4			1
Duckling Creek	18o25-2a	syenite	56.007961	-125.701574			178.9±1.3			1
Duckling Creek	18o24-1	syenite	56.012295	-125.681727				177±5		1
Duckling Creek	19GJ13-5a	syenite	55.999451	-125.526168			174.7±0.7			1
Duckling Creek	AD06-0552	vein: biotite-albite-apatite								1
Duckling Creek	MM106-9-7	leucosyenite dike			176.8±0.4					2
Duckling Creek	06FD626	vein: biotite-k-feldspar-albite-magnetite								2
Duckling Creek	06FD708	pegmatite dike			177.6±0.2					2
Duckling Creek	06FD654	K-feldspar megacrystic porphyry			178.8±0.2					2
Duckling Creek	06FD706	Equigranular monzonite			179.7±2.5					2
Duckling Creek	06FD838	Fine-grained, equigranular syenite			180.2±0.3					2
Duckling Creek	06FD709	biotite pyroxenite			178.4±0.3				181.7±1.0	2
Duckling Creek	07AB G7	syenite			178.6±0.2					3
Duckling Creek	07AB G3	rhythmically layered diopside syenite			178.6±0.2					3
Duckling Creek	07AB G2	syenite			178.7±0.3					3
Duckling Creek	07AB G5	syenite			177.3±0.4					3
Duckling Creek	07AB G1	pseudoleucite bearing feldspathic pyroxenite			178.4±0.3					3
Thane Creek	19GJ12-4	diorite	56.211666	-125.646053			206.6±0.9			1
Thane Creek	19GJ13-3	quartz monzodiorite	56.024407	-125.598711			194±1.1			1
Thane Creek	18o26-1	quartz monzodiorite	56.057991	-125.607348				202±5		1
Thane Creek	18o22-1d	diorite	56.013314	-125.820707				124±2	126±2	1
Thane Creek	18o22-1d	diorite	56.013314	-125.820707				124±1	124±1	1
Thane Creek	18o22-1a	hornblendite	56.013314	-125.820707			196.6±0.9			1
Thane Creek	FF91-5-3	CAT monzonite	56.013314	-125.820707			197.6±0.1			1
Thane Creek	06FD859	Rhonda Gabro			200.9±0.2					4
Notes: ± reported at 2s; <sup>a</sup> University of Alberta; <sup>aa</sup> University of British Columbia z-zircon; <sup>t</sup> titanite; <sup>hbl</sup> =hornblende; <sup>mv</sup> =muscovite										3
1-this study; 2-Devine et al. (2014); 3-Bath et al. (2014); 4-Mortensen et al. (1995)										

using conventional crushing, grinding, and Wilfley table techniques, followed by final concentration using heavy liquids and magnetic separations, then air-abrasion. Following dissolution of multi-grain zircon and titanite fractions in the presence of a  $^{233-235}\text{U}$ - $^{205}\text{Pb}$  tracer, isotopic ratios were measured using a modified single collector VG-54R thermal ionization mass spectrometer (TIMS) equipped with an analogue Daly photomultiplier. In 2020, these legacy raw data were re-reduced using the Excel-based program of Schmitz and Schoene (2007). Standard concordia diagrams were constructed, and weighted averages calculated with Isoplot (Ludwig, 2003). All errors are quoted at the  $2\sigma$  or 95% level of confidence.

### 3.2. Ar-Ar laser step-heating

This study presents  $^{40}\text{Ar}/^{39}\text{Ar}$  laser step-heating ages for single hornblende, muscovite, and biotite crystals. Samples were prepared at the British Columbia Geological Survey where they were crushed and sieved to between 100 and 250  $\mu\text{m}$  and run through a Frantz magnetic separator after which single crystals were handpicked under a binocular microscope. Full analytical techniques and supporting data are in Ootes et al. (2020c). Three of the biotite  $^{40}\text{Ar}/^{39}\text{Ar}$  laser step-heating results were also reported in Ootes et al. (2020b).

All  $^{40}\text{Ar}/^{39}\text{Ar}$  analytical work was performed at the University of Manitoba using a multi-collector Thermo Fisher Scientific ARGUSVI mass spectrometer linked to a stainless steel Thermo Fisher Scientific extraction/purification line and Photon Machines (55 W) Fusions 10.6  $\text{CO}_2$  laser. All specimens were irradiated in the cadmium-lined, in-core CLICIT facility of the Oregon State University TRIGA reactor. The duration of irradiation was 70 hours and was conducted with the Fish Canyon sanidine (28.201 Ma; Kuiper et al., 2008). Irradiated samples were placed in a Cu sample tray, with a KBr cover slip, in a stainless steel high-vacuum extraction line and baked with an infrared lamp for 24 hours. Single crystals were either fused or step heated using the laser, and reactive gases were removed after  $\sim 3$  minutes by three NP-10 SAES getters (two at room temperature and one at  $450^\circ\text{C}$ ) before being admitted to an ARGUSVI mass spectrometer by expansion. Five argon isotopes were measured simultaneously during a period of 6 minutes. Measured isotope abundances were corrected for extraction-line blanks, which were determined before every sample analysis. Each of the resulting steps have relatively small errors, and the integrated ages were calculated from the average and uncertainty by standard deviation of the best analysis.

## 4. Results

### 4.1. Thane Creek suite

#### 4.1.1. Thane Creek quartz diorite: 19GJ12-4, U-Pb zircon, 206.6 $\pm$ 0.9 Ma

The sample was taken 17.9 km east-northeast of Notch Peak (Fig. 2). It is a white and black, medium-grained, equigranular quartz diorite, and is composed of mostly plagioclase ( $\sim 62\%$ ), with about 25% equal parts of green amphiboles, with corroded

clinopyroxene cores, and brown (metamorphic?) and green biotite. The sample contains minor quartz ( $\sim 6\%$ ) and alkali feldspar ( $\sim 7\%$ ), with accessory magnetite, apatite, titanite, and epidote. Titanite occurs as rims on magnetite grains. Trace fine-grained chalcopyrite is disseminated and occurs as inclusions in magnetite.

After analysis and data reduction, two zircons were filtered out for exceeding  $\text{Ca} > 300$  ppm and  $\text{Ti} > 20$  ppm, and one zircon was rejected for  $f^{206}\text{Pb}_c > 1\%$ . Ten remaining analyses yield a weighted mean  $^{206}\text{Pb}/^{238}\text{U}$  date of  $206.6 \pm 0.9$  Ma (MSWD=1.77; probability of fit=0.07). This weighted mean is interpreted as the best estimate for the crystallization age (Figs. 5a, b).

#### 4.1.2. Thane Creek hornblende: 18lo22-1a, U-Pb zircon, CA-TIMS: 197.6 $\pm$ 0.1 Ma; LA-ICPMS: 191.4 $\pm$ 0.7 Ma

The sample was taken 18.6 km south-southeast of Mount Ferris (Fig. 2). It is a coarse-grained to pegmatitic plagioclase-bearing hornblende. Pegmatitic white hornblende-plagioclase segregations are interstitial to predominantly green hornblende. Hornblende is commonly overgrown by brown or green biotite, with biotite making up  $\sim 10\%$  of the sample. The sample contains  $\sim 5\%$  magnetite that is interstitial to amphibole and is concentrated with accessory titanite and apatite. Coarse, subhedral accessory epidote occurs in pegmatitic plagioclase segregations. Trace fine-grained chalcopyrite is disseminated through the sample.

Ootes et al. (2020b, c) report a  $197.6 \pm 0.1$  Ma zircon crystallization age, determined by chemical abrasion CA-TIMS (Fig. 5c). For LA-ICPMS, nine analyses were rejected for exceeding  $f^{206}\text{Pb}_c > 1\%$ . Thirty-three remaining zircons yield a  $^{206}\text{Pb}/^{238}\text{U}$  weighted mean date of  $191.4 \pm 0.7$  Ma (MSWD=0.87; probability of fit=0.68) (Figs. 5c, d). The discrepancy between the LA-ICP-MS weighted mean  $^{206}\text{Pb}/^{238}\text{U}$  date and the reported CA-TIMS  $^{206}\text{Pb}/^{238}\text{U}$  date ( $197.6 \pm 0.1$  Ma) may be due to differences in the calibration techniques between the LA-ICP-MS and CA-TIMS methods. Although we consider both the LA-ICP-MS and CA-TIMS U-Pb dates of the hornblende valid, the CA-TIMS date ( $197.6 \pm 0.1$  Ma) is interpreted to be more accurate and the best estimate of the crystallization age.

#### 4.1.3. Thane Creek diorite: 18lo22-1d, $^{40}\text{Ar}/^{39}\text{Ar}$ hornblende, biotite, 126-124 Ma

This sample is from 18.6 km south-southeast of Mount Ferris, 100 m east of the hornblende sample (18lo22-1a; section 4.1.2., Fig. 2). It is a 'salt and pepper', medium-grained equigranular diorite. The rock contains a moderate foliation defined by plagioclase, biotite, and amphibole. The sample is mostly clay-altered plagioclase (65%), biotite (12%), and amphibole (6%). Minor altered alkali feldspar (7%) and quartz (1-2%) are present, interstitial to plagioclase. Accessory anhedral to subhedral, fine-grained epidote, apatite, magnetite, and zircon occur with biotite. Trace fine-grained chalcopyrite is disseminated through the sample. Ootes et al. (2020b, c) report a  $196.6 \pm 0.9$  Ma zircon crystallization age, determined by CA-TIMS.

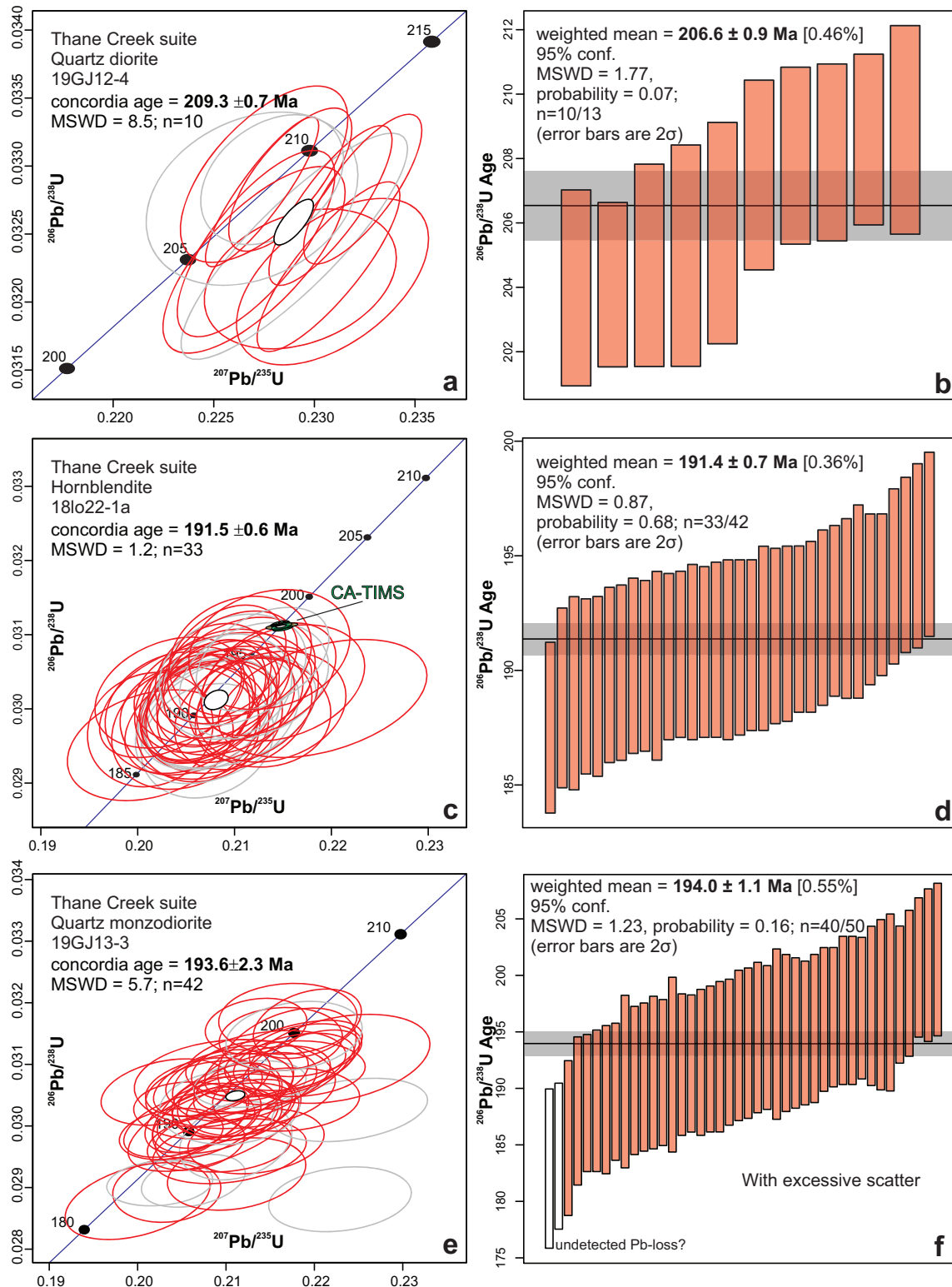


**Fig. 5.** Results of Thane Creek suite zircon U-Pb LA-ICP-MS analysis. Data used for weighted mean calculations have been filtered using the methods outlined in section 3.1.1. and Ootes et al. (2020c). Grey ellipses in concordia plots represent data that have been filtered and were not included in age calculations. Uncertainties are reported at the  $2\sigma$  or 95.5% confidence level. **a)** Concordia plot of quartz diorite sample 19GJ12-4. **b)** Weighted mean  $^{206}\text{Pb}/^{238}\text{U}$  date, interpreted as the crystallization age, of quartz diorite sample 19GJ12-4. **c)** Concordia plot of hornblende sample 18lo22-1a. Also plotted are CA-TIMS results (Ootes et al., 2020b, c). **d)** Weighted mean  $^{206}\text{Pb}/^{238}\text{U}$  date of hornblende sample 18lo22-1a. **e)** Concordia plot of quartz monzodiorite sample 19GJ13-3. **f)** Weighted mean  $^{206}\text{Pb}/^{238}\text{U}$  date of quartz monzodiorite sample 19GJ13-3, after applying excessive scatter constant (section 3.1.1.). Colourless bars passed the data filters outlined in section 3.1.1. but were not included in the weighted mean calculation due to the younger skew of these points, possibly indicating undetected Pb-loss in the zircon grains.

Two aliquots each of hornblende and biotite were analyzed by ICP-MS via laser step-heating. For biotite-aliquot 1, seven steps (C-I) released 99.98%  $^{39}\text{Ar}$  and yield an integrated  $^{40}\text{Ar}/^{39}\text{Ar}$  age of  $126 \pm 2$  Ma (Fig. 6a). For biotite-aliquot 2, six steps (D-I) released 80.23%  $^{39}\text{Ar}$  and yield an integrated  $^{40}\text{Ar}/^{39}\text{Ar}$  age of  $124 \pm 1$  Ma (Fig. 6b). For hornblende-aliquot 1, six steps (C-H) released 99.82%  $^{39}\text{Ar}$  and yield an integrated  $^{40}\text{Ar}/^{39}\text{Ar}$  age of  $124 \pm 2$  Ma (Fig. 6c). For hornblende-aliquot 2, ten steps (C-L) released 99.01%  $^{39}\text{Ar}$  and yield an integrated  $^{40}\text{Ar}/^{39}\text{Ar}$  age of  $124 \pm 1$  Ma (Fig. 6d).

#### 4.1.4. Thane Creek monzodiorite: 19GJ13-3, U-Pb zircon, $194.0 \pm 1.1$ Ma

This sample is from 25.9 km southeast of Notch Peak (Fig. 2). The sample is a ‘salt and pepper’, fine- to medium-grained, equigranular quartz monzodiorite, composed of ~40% euhedral plagioclase, ~30% poikilitic alkali feldspar, and ~15% anhedral, strained quartz. Mafic minerals make up ~10% of the sample, mainly subhedral amphibole (8%) with lesser biotite (2%). Anhedral magnetite and titanite, and euhedral apatite and zircon are accessory. Titanite occurs as ~1 mm grains and as fine rims on magnetite.

After LA-ICP-MS analyses, six zircons were rejected for  $f^{206}\text{Pb}_c > 1\%$ , two zircons were rejected for  $>5\%$  discordance. All remaining zircon passed the trace element filters, and no xenocrystic or antecrystic grains or cores were identified. An excess scatter constant of 3.99 was added to the standard error of the filtered data points to decrease the MSWD of weighted mean  $^{206}\text{Pb}/^{238}\text{U}$  date. The youngest two analyses were then rejected in order to further reduce the scatter, as they may indicate undetected Pb-loss. Forty remaining analyses yield a weighted mean  $^{206}\text{Pb}/^{238}\text{U}$  date of  $194.0 \pm 1.1$  Ma (MSWD=1.23; probability of fit=0.16). This weighted mean is interpreted as the best estimate for the crystallization age (Figs. 5e, f).

#### 4.1.5. Thane Creek monzodiorite: 18lo26-1, $^{40}\text{Ar}/^{39}\text{Ar}$ hornblende, $202 \pm 5$ Ma

The sample site is 23.2 km southeast of Notch Peak and 3.69 km north of sample 19GJ13-3 (section 4.1.4.; Fig. 2). This sample is of relatively pristine (unaltered) monzodiorite with euhedral hornblende and accessory euhedral magnetite and titanite. The sample yielded hornblende and eight steps (E-L) released 84.07%  $^{39}\text{Ar}$  and yield an integrated  $^{40}\text{Ar}/^{39}\text{Ar}$  age of  $202 \pm 5$  Ma (Fig. 6e).

### 4.2. Duckling Creek suite

#### 4.2.1. Duckling Creek syenite: 18lo25-2a, U-Pb zircon, $178.9 \pm 1.3$ Ma

Collected 22.7 km southeast of Notch Peak (Fig. 2), the sample is a pink-white, medium-grained, equigranular syenite. The sample consists of ~90% two alkali feldspars (K- and Na-bearing), with lesser clinopyroxene (~5%). Magnetite, titanite, chlorite, and zircon are accessory minerals. Titanite forms ~1 mm wide euhedral, wedge-shaped grains intergrown with clinopyroxene.

Two types of zircon were identified during mineral picking. The first type (18lo25-2a z1) are clear-pink coloured zircon fragments between 100 to 200  $\mu\text{m}$ . The second type (18lo25-2a z2) are larger grains (300 to 400  $\mu\text{m}$ ) that are brown with good crystal habit but with cores that are commonly metamict or highly fractured (see zircon CL images; Ootes et al., 2020c). Only type one zircons (z1) were considered in the U-Pb age interpretation as none of type two zircon (z2) LA-ICP-MS data passed the filters. Fourteen z1 and z2 zircons were rejected for  $>10\%$  discordance, four zircons were rejected for exceeding Fe  $>300$  ppm and/or Ca  $>300$  ppm and La  $>1$  ppm. One zircon was rejected for excessive standard error of Ca, and two zircons were rejected for high U and internal structures. An excess scatter constant of 3.11 was added to the standard error of the filtered data points to decrease the MSWD of the weighted mean  $^{206}\text{Pb}/^{238}\text{U}$  date. Twenty-two remaining type one zircons yield a weighted mean  $^{206}\text{Pb}/^{238}\text{U}$  date of  $178.9 \pm 1.3$  Ma (MSWD=1.33; probability of fit=0.15). This weighted mean is interpreted as the best estimate for the crystallization age (Figs. 7a-e).

#### 4.2.2. Duckling Creek syenite: 18lo24-1, $^{40}\text{Ar}/^{39}\text{Ar}$ hornblende, $177 \pm 5$ Ma

This sample is of coarse-grained equigranular monzonite (syenite) from the centre of the Duckling Creek suite, 23.9 km south of Mount Ferris, 1.33 km northeast of sample 18lo25-2a (section 4.2.1., Fig. 2). The sample consists of coarse K-feldspar (80%) with 15% mafic minerals. These are mostly medium-grained green clinopyroxene with lesser dark-green amphibole. Medium-grained titanite is intergrown with clinopyroxene and accessory magnetite is disseminated throughout. The sample was collected 1.33 km northeast of sample 18lo25-2a (section 4.2.1.) and was used for Ar-Ar step-heating as sample 18lo25-2a did not yield hornblende. For hornblende, four steps (F-I) released 98.45%  $^{39}\text{Ar}$  and yield an integrated  $^{40}\text{Ar}/^{39}\text{Ar}$  age of  $177 \pm 5$  Ma (Fig. 8).

#### 4.2.3. Duckling Creek syenite: 19GJ13-5a, U-Pb zircon, $174.7 \pm 0.7$ Ma

The sample was collected 31.1 km southwest of Notch Peak (Fig. 2), next to the Slide Cu-Au porphyry prospect and 7 m south of a grab sample with chalcopyrite that yielded 0.07 wt.% Cu (19GJ13-5b; Ootes et al., 2020b). The sample is a pink-white and greenish black, medium-grained, equigranular syenite. It contains alkali feldspar (~70%), with lesser amphibole (9%), plagioclase (8%), and clinopyroxene (5%). Biotite, chlorite, and magnetite combine to make up ~5% of the sample, whereas fine-grained apatite, titanite, epidote, and zircon are accessory minerals. Chalcopyrite forms rare fine, disseminated grains, and may be rimmed by titanite.

Two zircon U-Pb analyses were rejected for  $f^{206}\text{Pb}_c > 1\%$ , whereas the remaining analyses passed all data filters. Twenty-four remaining analyses yield a weighted mean  $^{206}\text{Pb}/^{238}\text{U}$  date of  $174.7 \pm 0.7$  Ma (MSWD=1.36; probability of fit=0.12). The weighted mean is interpreted as the best estimate for the crystallization age (Fig. 9).

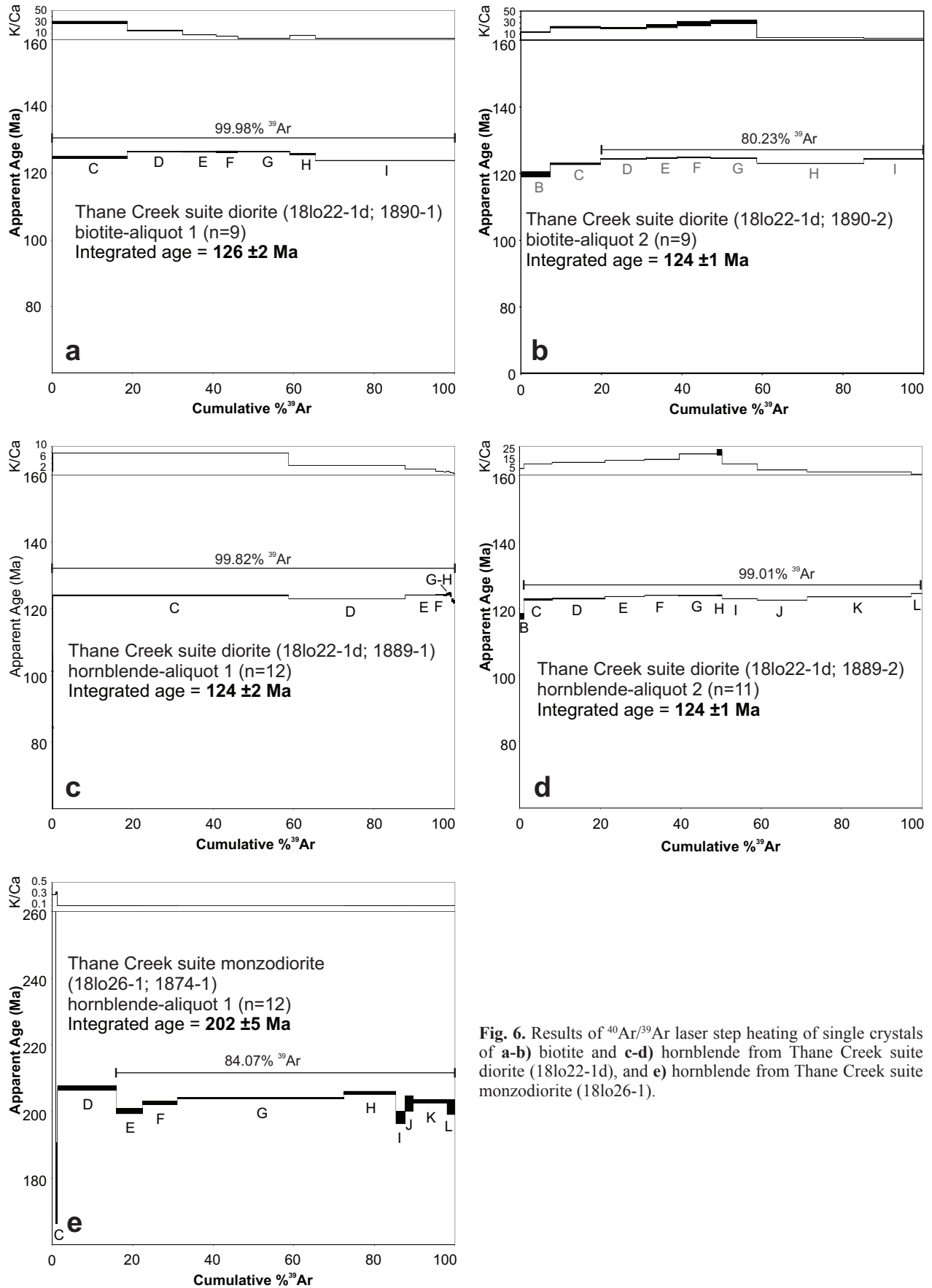


**Fig. 6.** Results of  $^{40}\text{Ar}/^{39}\text{Ar}$  laser step heating of single crystals of **a-b)** biotite and **c-d)** hornblende from Thane Creek suite diorite (18lo22-1d), and **e)** hornblende from Thane Creek suite monzodiorite (18lo26-1).

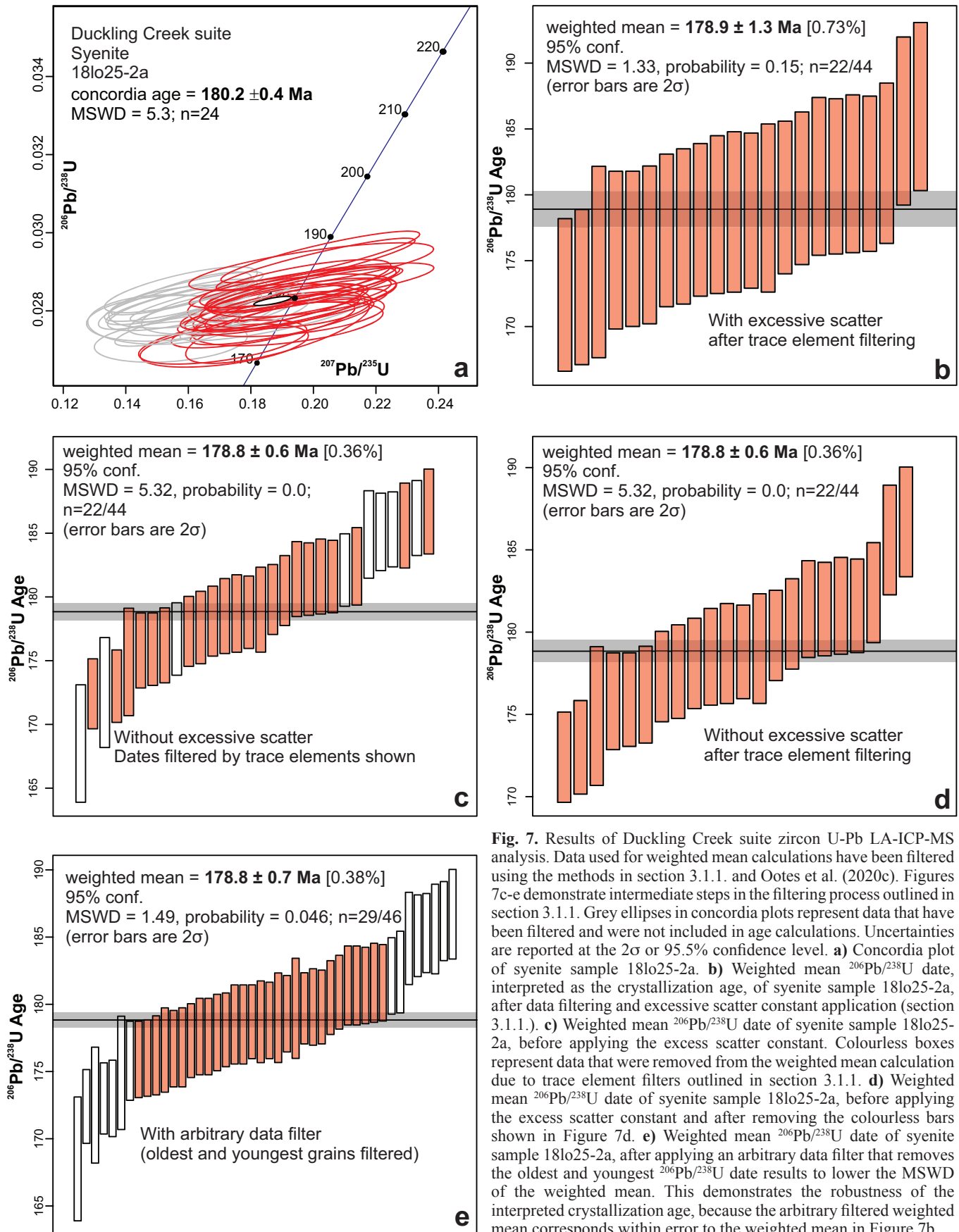


**Fig. 7.** Results of Duckling Creek suite zircon U-Pb LA-ICP-MS analysis. Data used for weighted mean calculations have been filtered using the methods in section 3.1.1. and Ootes et al. (2020c). Figures 7c-e demonstrate intermediate steps in the filtering process outlined in section 3.1.1. Grey ellipses in concordia plots represent data that have been filtered and were not included in age calculations. Uncertainties are reported at the  $2\sigma$  or 95.5% confidence level. **a)** Concordia plot of syenite sample 18lo25-2a. **b)** Weighted mean  $^{206}\text{Pb}/^{238}\text{U}$  date, interpreted as the crystallization age, of syenite sample 18lo25-2a, after data filtering and excessive scatter constant application (section 3.1.1.). **c)** Weighted mean  $^{206}\text{Pb}/^{238}\text{U}$  date of syenite sample 18lo25-2a, before applying the excess scatter constant. Colourless boxes represent data that were removed from the weighted mean calculation due to trace element filters outlined in section 3.1.1. **d)** Weighted mean  $^{206}\text{Pb}/^{238}\text{U}$  date of syenite sample 18lo25-2a, before applying the excess scatter constant and after removing the colourless bars shown in Figure 7d. **e)** Weighted mean  $^{206}\text{Pb}/^{238}\text{U}$  date of syenite sample 18lo25-2a, after applying an arbitrary data filter that removes the oldest and youngest  $^{206}\text{Pb}/^{238}\text{U}$  date results to lower the MSWD of the weighted mean. This demonstrates the robustness of the interpreted crystallization age, because the arbitrary filtered weighted mean corresponds within error to the weighted mean in Figure 7b.

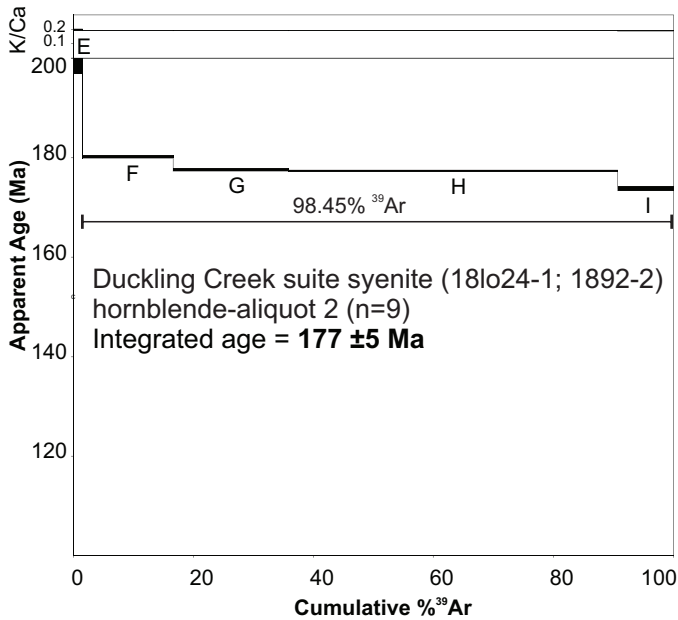


Fig. 8. Results of  $^{40}\text{Ar}/^{39}\text{Ar}$  laser step heating of a single crystal of hornblende from Duckling Creek syenite (18lo24-1).

### 4.3. Osilinka suite

#### 4.3.1. Osilinka granite: 18lo17-1, U-Pb zircon 159.2 ± 4 Ma (maximum), $^{40}\text{Ar}/^{39}\text{Ar}$ muscovite, 122 ± 5 Ma, biotite, 116 ± 1 Ma

We collected this sample 11.9 km southeast of Notch Peak (Fig. 2). The sample is of a white (leucocratic), medium-grained, equigranular granite. Strained quartz (~37%), subhedral alkali feldspar (32%), and subhedral plagioclase (26%) comprise most of the sample. Rare accessory biotite,

muscovite, and magnetite constitute less than 5% of the rock. Fine-grained biotite and magnetite occur interstitial to feldspar grains, whereas muscovite and sericite are present within feldspar cores and along grain boundaries.

Eight zircon U-Pb isotopes analyses were rejected for  $f^{206}\text{Pb}_c > 1\%$  and/or  $> 10\%$  discordance, and one zircon was rejected for  $\text{Fe} > 300$  ppm. The thirteen remaining zircon yield an approximately 30 million year spread in  $^{206}\text{Pb}/^{238}\text{U}$  dates, and are interpreted as inherited. The youngest zircon has a  $^{206}\text{Pb}/^{238}\text{U}$  date of  $159.2 \pm 4$  Ma; it is unclear if this is a magmatic or inherited zircon and therefore the  $^{206}\text{Pb}/^{238}\text{U}$  date is interpreted as the maximum crystallization age (Fig. 10a).

Both muscovite and biotite were separated from the sample and tested by laser step heating. For muscovite six steps (D-I) released 85.83%  $^{39}\text{Ar}$  and yield an integrated  $^{40}\text{Ar}/^{39}\text{Ar}$  age of  $122 \pm 5$  Ma (Fig. 11a). For biotite five steps (C-G) released 57.98%  $^{39}\text{Ar}$  and yield an integrated  $^{40}\text{Ar}/^{39}\text{Ar}$  age of  $116 \pm 1$  Ma (Fig. 11b).

#### 4.3.2. Sheet cutting Osilinka granite, 18lo20-4, U-Pb zircon, 162.2 ± 2.6 Ma (maximum)

The sample is from a flat-lying sheet, at least 4 m thick, that cuts Osilinka suite rocks, 14.01 km southeast of Notch Peak (Fig. 2). Fine-grained plagioclase and quartz make up most of the groundmass, with plagioclase phenocrysts up to 0.5 cm. Magnetite, chlorite, epidote, and calcite are accessory in the groundmass. A ~0.5 mm wide calcite-filled vein cuts the sample. Rare, ~2.5 mm wide euhedral chalcopyrite grains are in the groundmass. Eight zircon U-Pb analyses were rejected for  $f^{206}\text{Pb}_c > 1\%$  and/or  $> 10\%$  discordance. The nine remaining zircon yield an approximately 100 million year spread in  $^{206}\text{Pb}/^{238}\text{U}$  dates and are interpreted as inherited. The

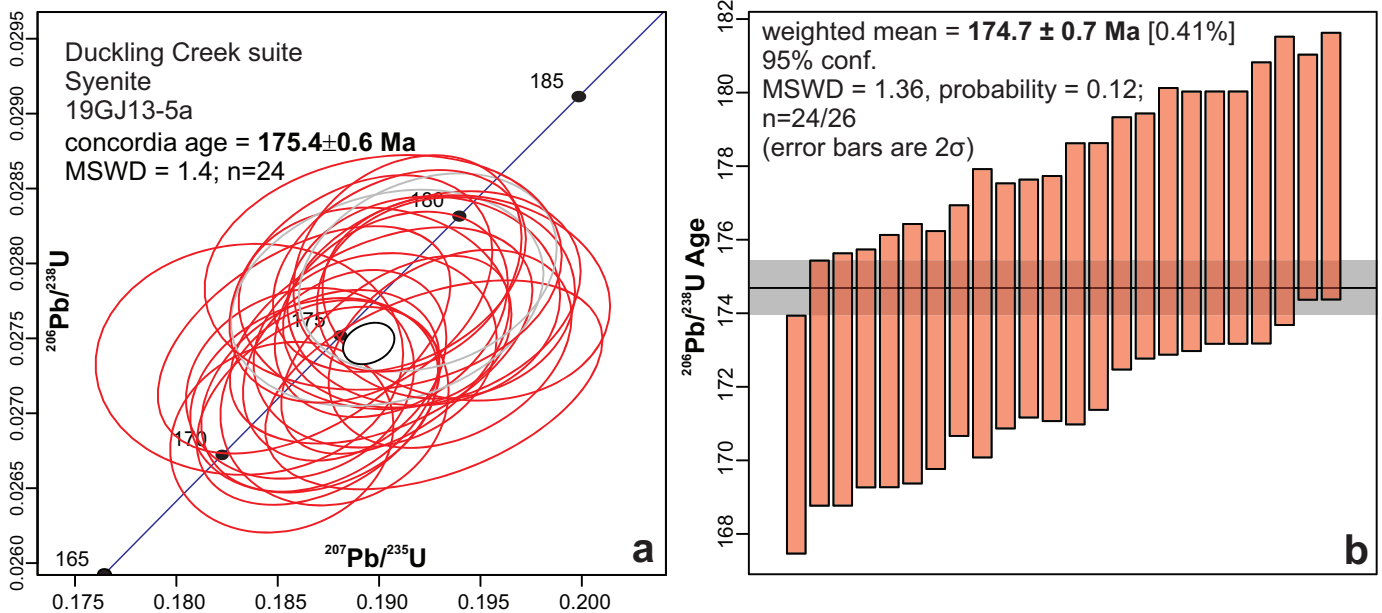
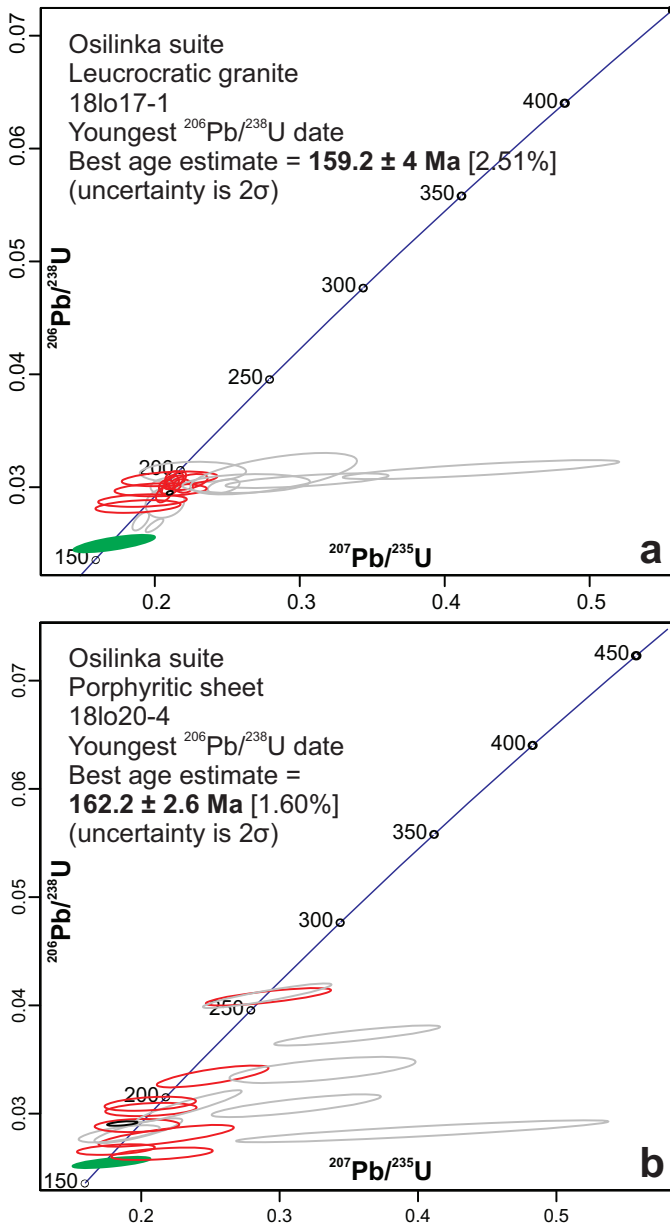
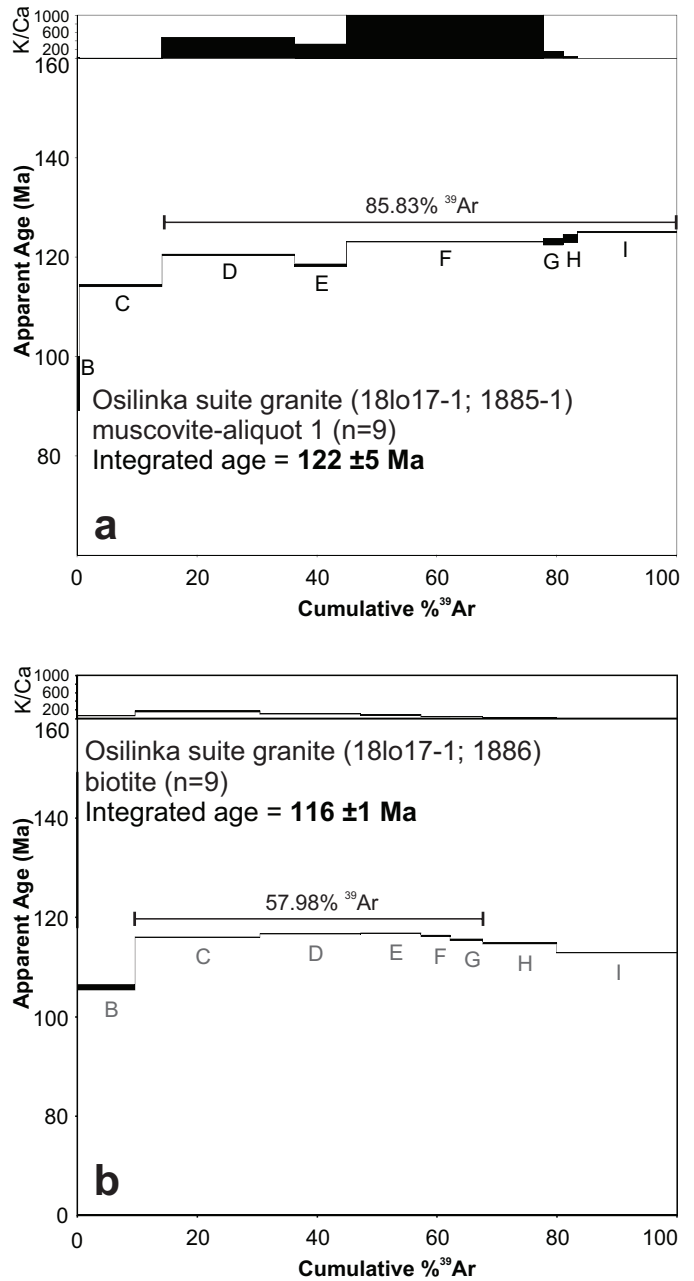


Fig. 9. Results of Duckling Creek suite zircon U-Pb LA-ICP-MS analysis. **a)** Concordia plot of syenite sample 19GJ13-5a. **b)** Weighted mean  $^{206}\text{Pb}/^{238}\text{U}$  date, interpreted as the crystallization age, of syenite sample 19GJ13-5a.



**Fig. 10.** Results of Osilinka suite zircon U-Pb LA-ICP-MS analysis. Grey ellipses in concordia plots represent data that have been filtered (section 3.1.1.) and were not included in age calculations. Uncertainties are reported at the  $2\sigma$  or 95.5% confidence level. **a)** Concordia plot of granite sample 18lo17-1. The green ellipse is the youngest zircon result, interpreted as the maximum age. Red ellipses are data that passed the data filters in section 3.1.1. and the zircon grains are interpreted as antecrysts or xenocrysts. **b)** Concordia plot of porphyritic sheet sample 18lo20-4. The green ellipse is the youngest zircon result, interpreted as the maximum age. Red ellipses are data that passed the filters in section 3.1.1. and the zircon grains are interpreted as antecrysts or xenocrysts.

youngest zircon has a  $^{206}\text{Pb}/^{238}\text{U}$  date of  $162.2 \pm 2.6 \text{ Ma}$ ; it is unclear if this is a magmatic or inherited zircon and therefore the  $^{206}\text{Pb}/^{238}\text{U}$  date is interpreted as the maximum crystallization age (Fig. 10b).



**Fig. 11.** Results of  $^{40}\text{Ar}/^{39}\text{Ar}$  laser step heating of single crystals of **a)** muscovite and **b)** biotite from Osilinka suite granite (18lo17-1).

#### 4.4. Mesilinka suite

##### 4.4.1. Mesilinka tonalite: 19GJ12-1, U-Pb zircon, $134.1 \pm 0.5 \text{ Ma}$

We collected this sample 2.45 km northwest of Horn Peak (Fig. 2). It is a grey, medium-grained, equigranular biotite-rich tonalite with a foliation defined by biotite. Equigranular granite dikes cut the tonalite at an outcrop ~50 m away. The sample is composed of slightly altered plagioclase (~50%), with lesser strained quartz (~30%) and brown and green biotite (~15%). Subhedral amphibole and magnetite, anhedral epidote, apatite, and titanite, and euhedral zircon are accessory and spatially associated with patches of biotite.

Trace element concentrations were not analyzed and not used to filter the data, because insufficient zircon remained after LA-ICP-MS U-Pb and Lu-Hf analyses and the grains were too small (<60  $\mu\text{m}$  wide) for LASS mode. Three zircon U-Pb analyses were rejected for  $f^{206}\text{Pb}_c > 1\%$ . Two analyses were rejected from the age calculation because the zircons are interpreted as xenocrysts or antecrysts due to dark cores and disrupted rim growth in CL images (Ootes et al., 2020c). In addition, the zircons have elevated  $\delta^{18}\text{O}$  values relative to the other zircons (G. Jones, unpublished data, 2021). Eighteen remaining analyses yield a weighted mean  $^{206}\text{Pb}/^{238}\text{U}$  date of  $134.1 \pm 0.5$  Ma (MSWD=1.48; probability of fit=0.09). The weighted mean is interpreted as the best estimate for the crystallization age of this sample (Figs. 12a, b).

#### 4.4.2. Mesilinka tonalite: 18bg17-10, $^{40}\text{Ar}/^{39}\text{Ar}$ biotite, $108 \pm 2$ Ma and $111 \pm 3$ Ma

The sample was collected from 6.87 km south-southeast of Mount Ferris (Fig. 2), within a body of medium-grained tonalite that contains a foliation. It consists of 65% quartz and plagioclase with 30% mafic minerals. The mafic minerals are mostly green and lesser brown (metamorphic?) biotite and lesser euhedral hornblende. Titanite is an accessory mineral.

Two aliquots of biotite were analyzed by laser step-heating. For biotite-aliquot 1, six steps (E-J) released 99.66%  $^{39}\text{Ar}$  and yield an integrated  $^{40}\text{Ar}/^{39}\text{Ar}$  age of  $108 \pm 2$  Ma (Fig. 13a). For biotite-aliquot 2, ten steps (B-M; steps E and H not included) released 99.98%  $^{39}\text{Ar}$  and yield an integrated  $^{40}\text{Ar}/^{39}\text{Ar}$  age of  $111 \pm 3$  Ma (Fig. 13b).

#### 4.4.3. Mesilinka granodiorite: 18lo19-2, $^{40}\text{Ar}/^{39}\text{Ar}$ biotite, $123 \pm 2$ Ma

This sample, a medium-grained equigranular granodiorite with biotite and minor hornblende, was collected 8.77 km south of Mount Ferris (Fig. 2). The sample yielded biotite and six Ar-release steps (B-H) released 77.07%  $^{39}\text{Ar}$ , yielding an integrated  $^{40}\text{Ar}/^{39}\text{Ar}$  age of  $123 \pm 2$  Ma (Fig. 13c).

#### 4.4.4. Mesilinka K-feldspar porphyritic granite: 18lo12-7, U-Pb zircon, $134.8 \pm 1.2$ Ma, $^{40}\text{Ar}/^{39}\text{Ar}$ biotite, $112 \pm 3$ Ma

The sample, a medium-grained K-feldspar porphyritic granite with a foliation defined by biotite was collected 2.1 km northeast of Horn Peak (Fig. 2). Clay-altered alkali feldspar phenocrysts up to 5 cm (38%), strained anhedral quartz (28%), and myrmekitic plagioclase (22%) comprise most of the sample. Biotite (10%) is 1-2 mm wide and interstitial to feldspar and quartz. Accessory minerals include zircon, magnetite, apatite, epidote, and allanite with epidote rims.

From the LA-ICP-MS results, six analyses were rejected for  $f^{206}\text{Pb}_c > 1\%$  and/or  $> 10\%$  discordance. Ten analyses were rejected for exceeding Ca  $> 300$  ppm, Fe  $> 300$  ppm, and/or La  $> 1$  ppm. One analysis was identified as a xenocryst because the CL image (zircon 49, sample 18lo12-7; Ootes et al., 2020c) shows that the zircon has a bright rounded core that is crosscut by later growth zoning. For the remaining zircon, an excess

scatter constant of 2.68 was added to the standard error of the filtered data points to decrease the MSWD of the weighted mean  $^{206}\text{Pb}/^{238}\text{U}$  date. Fourteen zircons yield a weighted mean  $^{206}\text{Pb}/^{238}\text{U}$  date of  $134.8 \pm 1.2$  Ma (MSWD=1.64; probability of fit=0.07). The weighted mean is interpreted as the best estimate for the crystallization age of this sample (Figs. 12c, d).

This sample yielded biotite and eight steps (B-I) released 99.98%  $^{39}\text{Ar}$ , resulting in an integrated  $^{40}\text{Ar}/^{39}\text{Ar}$  age of  $112 \pm 3$  Ma (Fig. 13d).

#### 4.4.5. Mesilinka equigranular granite: 18lo11-1, U-Pb zircon, $127.9 \pm 0.8$ Ma

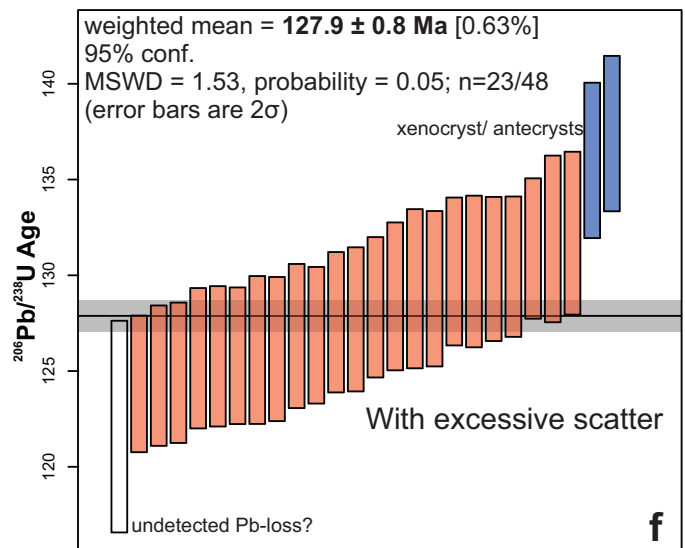
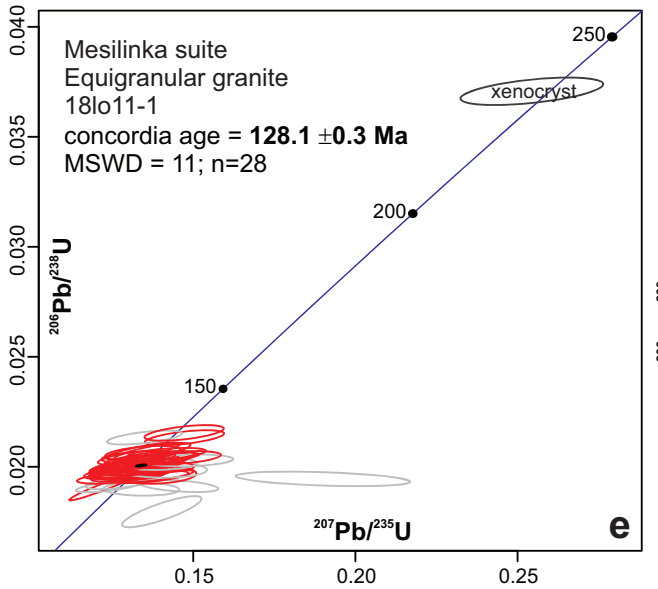
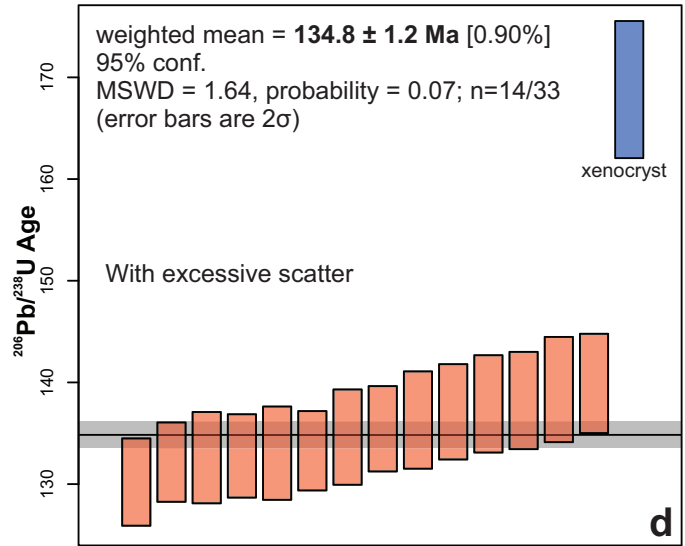
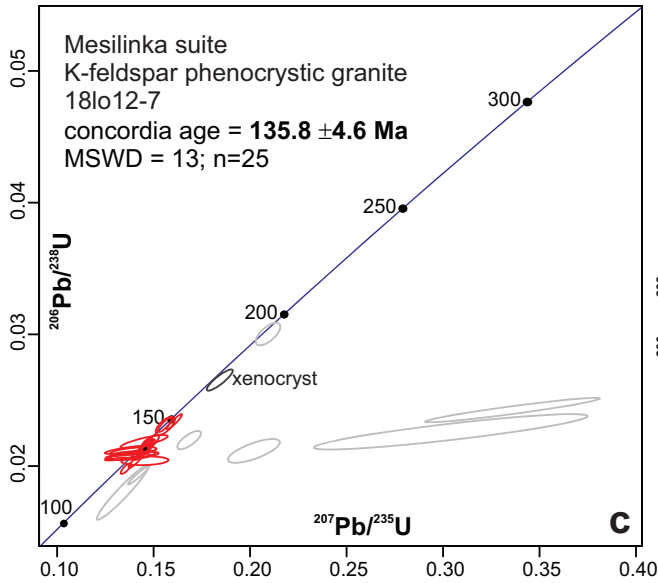
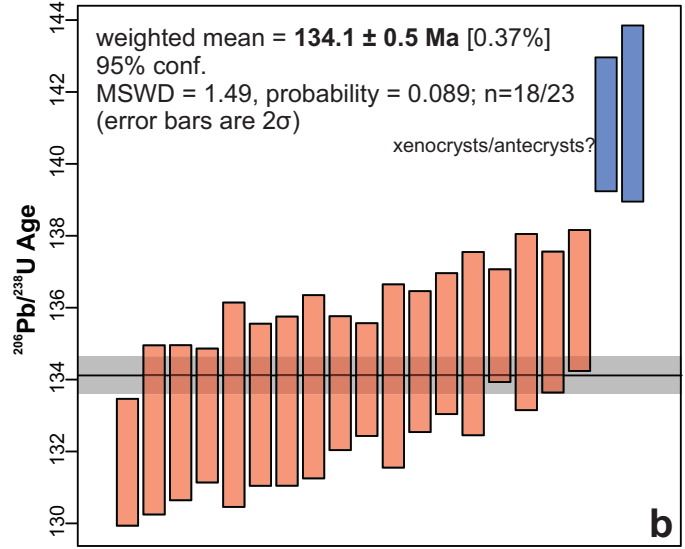
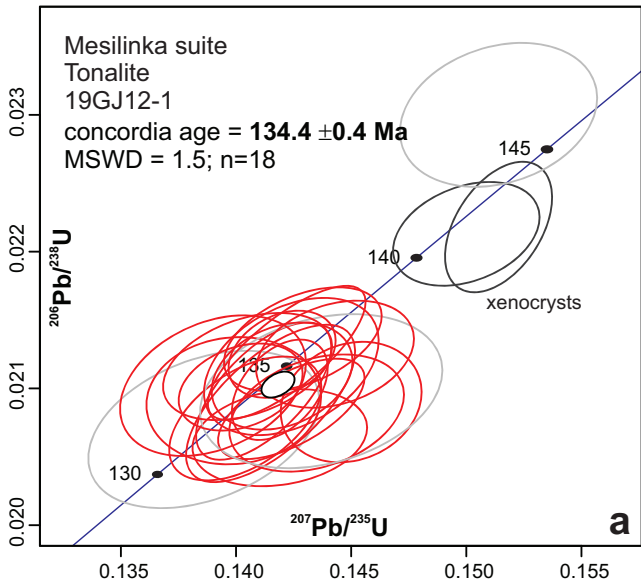
The sample, an equigranular, fine to medium-grained granite with a foliation defined by biotite was collected 1.48 km northeast of Horn Peak (Fig. 2). It consists mostly of strained fine-grained quartz (40%), anhedral medium-grained alkali feldspar (30%), and clay-altered plagioclase (25%). Accessory minerals include zircon, fine-grained muscovite, biotite, and magnetite. Magnetite may be rimmed by titanite.

Six analyses were rejected for  $f^{206}\text{Pb}_c > 1\%$  and/or  $> 10\%$  discordance. Thirteen analyses were rejected for exceeding La  $> 1$  ppm and/or Fe  $> 300$  ppm. Three zircons were rejected; one zircon (shown in Fig. 11e, not shown in Fig. 11f) and two other zircons are interpreted as antecrysts/xenocrysts because the CL images (zircons 8, 22, and 35 in sample 18lo11-1; Ootes et al., 2020c) show bright zircon cores that are crosscut by darker rims. For the remaining analyses, an excess scatter constant of 2.34 was added to the standard error of the filtered data points to decrease the MSWD of the weighted mean  $^{206}\text{Pb}/^{238}\text{U}$  date. The youngest zircon date was rejected due to possible undetected Pb-loss and large error in the  $^{206}\text{Pb}/^{238}\text{U}$  value. Twenty-three remaining analyses yield a weighted mean  $^{206}\text{Pb}/^{238}\text{U}$  date of  $127.9 \pm 0.8$  Ma (MSWD=1.53; probability of fit=0.05). The weighted mean is interpreted as the best estimate for the crystallization age of this sample (Figs. 12e, f).

#### 4.4.6. Mesilinka equigranular granite: 04PSC-277, U-Pb multi-grain titanite, $133.9 \pm 0.3$ Ma

The sample was collected from the north end of Hogem batholith, 21.5 km north-northwest of Horn Peak (Fig. 2). It is a medium-grained granite with ~55% feldspar (plagioclase>K-feldspar), 25% quartz, and 20% variably chloritized mafic minerals (biotite>hornblende) and is isotropic to weakly lineated.

Single zircon and multi-grain titanite fractions were analyzed by ID-TIMS. Two titanite fractions yield a weighted mean  $^{206}\text{Pb}/^{238}\text{U}$  date of  $133.9 \pm 0.3$  Ma (MSWD=1.15; Fig. 12g), interpreted as a minimum crystallization age estimate for the granitoid, because they record cooling through the titanite closure temperature of ca. 600-650°C (Flowers et al., 2005). Three zircon fractions that give significantly younger results than the titanites and are interpreted to have suffered from Pb-loss. One zircon fraction gives older, discordant results, likely due to the presence of inherited components.



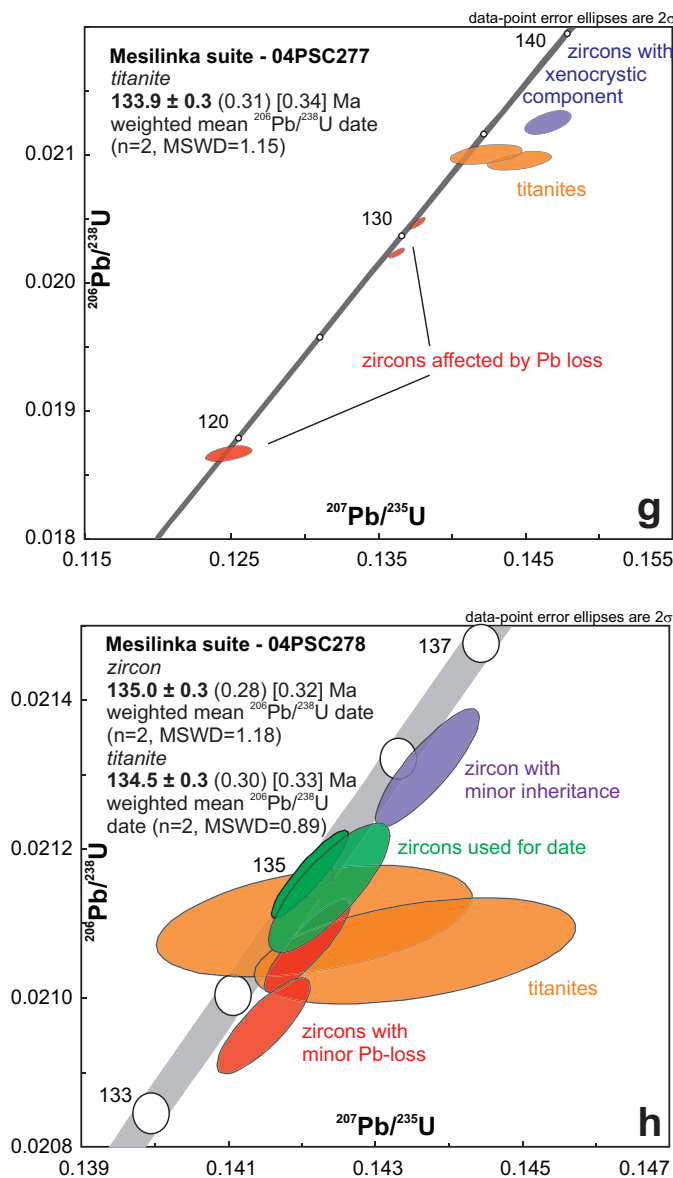


**Fig. 12.** Results of Mesilinka suite zircon U-Pb LA-ICP-MS analysis. Data used for weighted mean calculations have been filtered using the methods outlined in section 3.1.1. and Ootes et al. (2020c). Grey ellipses in concordia plots represent data that have been filtered and were not included in age calculations. Uncertainties are reported at the  $2\sigma$  or 95.5% confidence level. **a)** Concordia plot of tonalite sample 19GJ12-1. Dark grey ellipses passed the data filters in section 3.1.1., but are interpreted as antecrystic or xenocrystic zircon grains, and were not included in the concordia age calculation. **b)** Weighted mean  $^{206}\text{Pb}/^{238}\text{U}$  date, interpreted as the crystallization age, of tonalite sample 19GJ12-1. Blue bars are zircons interpreted as antecrysts or xenocrysts and were not included in the weighted mean calculation. **c)** Concordia plot of K-feldspar porphyritic granite sample 18lo12-7. The dark grey ellipse passed the data filters in section 3.1.1. but is interpreted as xenocrystic and not included in the age calculation. **d)** Weighted mean  $^{206}\text{Pb}/^{238}\text{U}$  date of K-feldspar porphyritic granite sample 18lo12-7, after applying excessive scatter constant (section 3.1.1.). The blue bar is an interpreted xenocrystic zircon and is not included in the weighted mean calculation. **e)** Concordia plot of equigranular granite sample 18lo11-1. The dark grey ellipse passed the data filters in section 3.1.1. but is interpreted as xenocrystic and is not included in the age calculation. **f)** Weighted mean  $^{206}\text{Pb}/^{238}\text{U}$  date of equigranular granite sample 18lo11-1, after applying excessive scatter constant (section 3.1.1.). The blue bars are interpreted antecrystic or xenocrystic zircons and are not included in the weighted mean calculation. The colourless bar passed the data filters in section 3.1.1. but was not included in the weighted mean calculation due to the large uncertainty and younger age, possibly indicating undetected Pb-loss in the zircon. **g)** Concordia plot of equigranular granite sample 04PSC277. Two titanite fractions were used to determine the weighted mean  $^{206}\text{Pb}/^{238}\text{U}$  date, interpreted as the crystallization age of this sample. **h)** Concordia plot of K-feldspar porphyritic granite sample 04PSC278. Two titanite and two zircon fractions yield overlapping weighted mean  $^{206}\text{Pb}/^{238}\text{U}$  dates, interpreted as the crystallization age of this sample.

#### 4.4.7. Mesilinka K-feldspar porphyritic granite: 04PSC-278, U-Pb zircon, $135.0 \pm 0.3$ Ma, U-Pb multi-grain titanite, $134.5 \pm 0.3$ Ma

The sample is from the north end of Hogem batholith, 22 km north-northwest of Horn Peak, and 1 km west of sample 04PSC-277 (section 4.4.6.; Fig. 2). The granite is coarse grained and porphyritic, with 30% K-feldspar (10% as 1 to 2 cm phenocrysts), 30% plagioclase, 20% quartz, and 20% chloritized mafic minerals (biotite >> hornblende). The sample has a strong lineation defined by elongate biotite clots and stretched feldspar and quartz grains, and a less-pronounced northeast-dipping tectonic foliation.

Single zircon and multi-grain titanite fractions were analyzed by ID-TIMS. Results for two overlapping and concordant zircon fractions give a weighted mean  $^{206}\text{Pb}/^{238}\text{U}$  date of  $135.0 \pm 0.3$  Ma (MSWD=0.18; Fig. 12h), interpreted

as a good estimate for the age of crystallization. Two slightly younger zircon fractions appear to have undergone minor Pb-loss. One zircon fraction is slightly older, likely due to the presence of inherited, or possibly or antecrystic components. Two titanite fractions yield a weighted mean  $^{206}\text{Pb}/^{238}\text{U}$  date of  $134.5 \pm 0.3$  Ma (MSWD=0.89; Fig. 12h), which overlaps with the interpreted crystallization age based on two zircon fractions and is consistent with cooling through the titanite closure temperature soon after emplacement.

## 5. Summary

Uranium-lead and  $^{40}\text{Ar}/^{39}\text{Ar}$  geochronology of Hogem batholith samples yield a range of crystallization ages from  $206.6 \pm 0.9$  to  $127.9 \pm 0.8$  Ma (Figs. 5-14; Table 1). The geochronological and geochemical attributes indicate a punctuated, protracted, and petrologically diverse intrusive

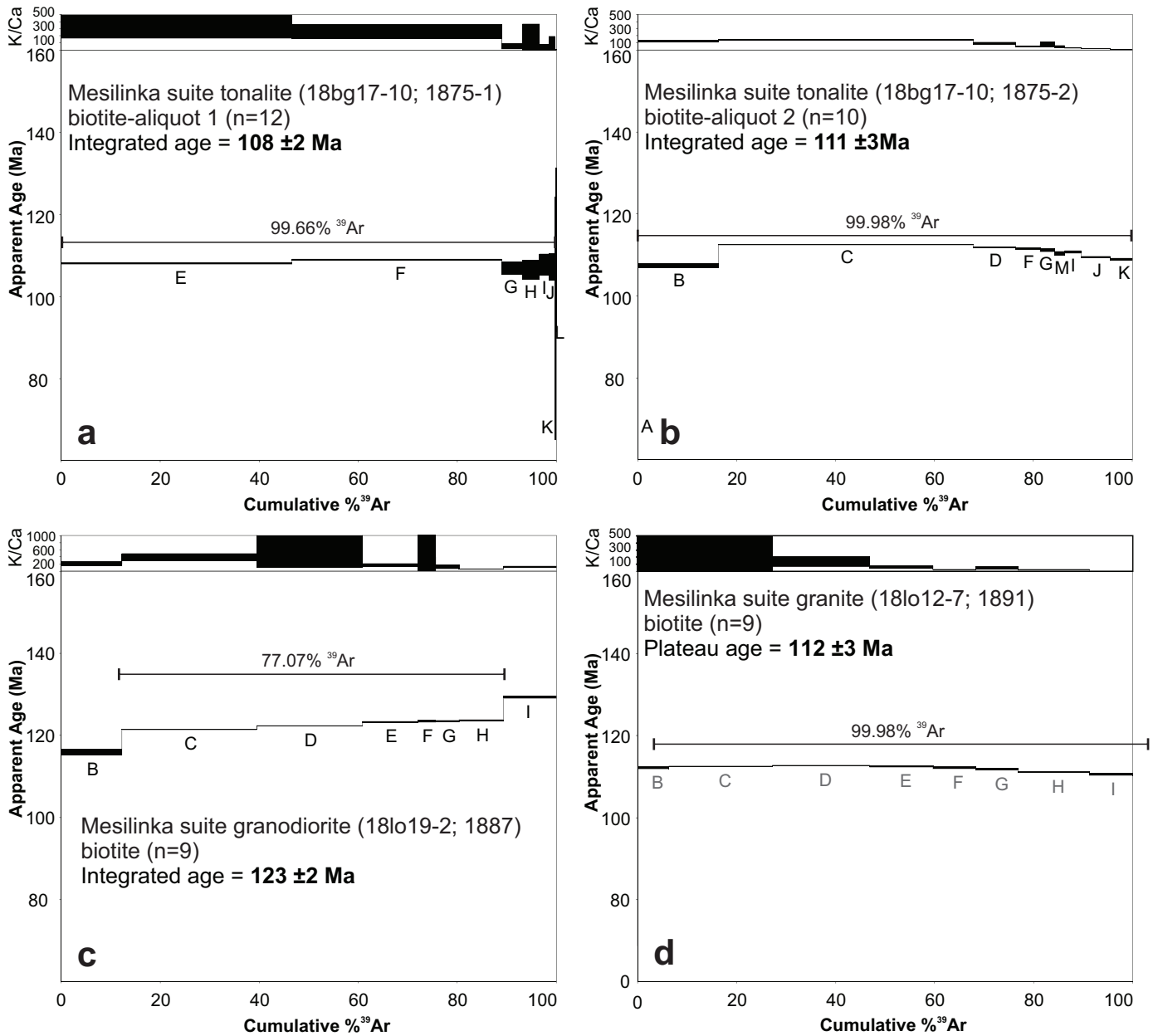


**Fig. 13.** Results of  $^{40}\text{Ar}/^{39}\text{Ar}$  laser step heating of single crystals of **a-b**) biotite from Mesilinka suite tonalite (18bg17-10), **c**) biotite from Mesilinka suite granodiorite (18lo19-2), and **d**) biotite from Mesilinka suite granite (18lo12-7).

history for the batholith (Figs. 3, 4, 14; Table 1). The Thane Creek suite crystallized between  $206.6 \pm 0.9$  and  $194 \pm 1.1$  Ma and a single  $^{40}\text{Ar}/^{39}\text{Ar}$  amphibole result from an undeformed quartz diorite phase indicates post-intrusion cooling at  $202 \pm 5$  Ma. The crystallization ages overlap an age of  $200.9 \pm 0.2$  Ma from the Rhonda-Dorothy gabbro in southern Hogem batholith (Devine et al., 2014) and a less-precise age of ca. 204 Ma from the CAT monzonite (Fig. 2, 14; Mortensen et al., 1995). The results of  $^{40}\text{Ar}/^{39}\text{Ar}$  amphibole and biotite from a deformed Thane Creek diorite indicate these minerals were reset during deformation after Duckling Creek suite emplacement ( $<175$  Ma) and underwent prolonged post-deformation cooling at ca. 125 Ma

synchronous with the Mesilinka suite (Figs. 6a-e, 14).

The Duckling Creek samples investigated in this study crystallized between  $178.9 \pm 1.3$  to  $174.7 \pm 0.7$  Ma (Figs. 7, 9, 14). A hornblende  $^{40}\text{Ar}/^{39}\text{Ar}$  age of  $177 \pm 5$  Ma, from a Duckling Creek suite syenite approximates the time of relatively rapid post-crystallization cooling (Figs. 8, 14). The full collection of results overlaps previously reported U-Pb and  $^{40}\text{Ar}/^{39}\text{Ar}$  results from the Lorraine Cu-Au deposit in southern Hogem batholith (Fig. 14; Bath et al., 2014; Devine et al., 2014). The  $174.7 \pm 0.7$  Ma zircon crystallization age result in this study is from a syenite sample that hosts Cu-mineralization (assay sample 19GJ13-5b; Ootes et al., 2020b) and is adjacent to

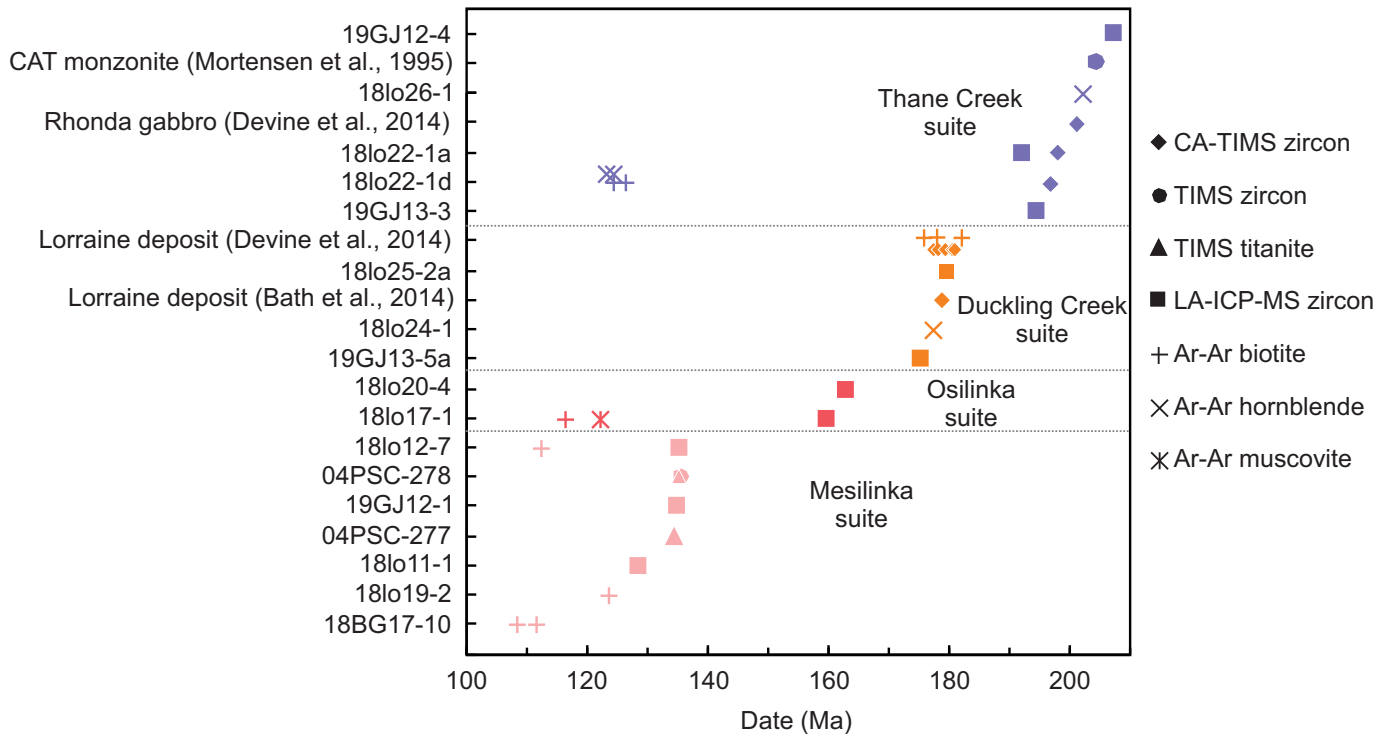


**Fig. 14.** Geochronology results of the four Hogem batholith intrusive suites. Data includes zircon U-Pb dates by CA-TIMS, TIMS, and LA-ICP-MS analysis, titanite U-Pb dates by TIMS analysis, and biotite, muscovite, and hornblende  $^{40}\text{Ar}/^{39}\text{Ar}$  dates by laser step-heating. The CAT monzonite zircon U-Pb date is from Mortensen et al. (1995). Data from Devine et al. (2014) includes CA-TIMS zircon U-Pb dates and biotite  $^{40}\text{Ar}/^{39}\text{Ar}$  dates of several samples from Duckling Creek suite phases in the Lorraine deposit area. Data from Bath et al. (2014) are represented as a single point, the average of five overlapping CA-TIMS zircon U-Pb dates of Duckling Creek suite samples from the Lorraine deposit area.

(or part of) the Slide Cu showing. This may indicate some Cu-mineralization within the Duckling Creek suite is slightly younger than at the Lorraine deposit (ca. 175 Ma; cf. 180-178.5 Ma, Bath et al., 2014; Devine et al., 2014), or may be due to results from different analytical techniques.

The Osilinka suite has a maximum crystallization age of ca. 160 Ma, estimated from the youngest zircon result of the Osilinka granite sample 18lo17-1 analysis ( $159.2 \pm 4$  Ma). A plagioclase-phenocrystic sheet cuts the Osilinka granite and yielded an overlapping U-Pb zircon date ( $162.2 \pm 2.6$  Ma). Results from  $^{40}\text{Ar}/^{39}\text{Ar}$  muscovite ( $122 \pm 5$  Ma) and biotite ( $116 \pm 1$  Ma) are interpreted as the time of post-deformation cooling (Figs. 11, 14).

The oldest tonalitic phase of the Mesilinka suite crystallized at  $134.1 \pm 0.5$  Ma and the youngest granite phase crystallized at  $127.9 \pm 0.8$  Ma (Figs. 12a-f, 14). Three Mesilinka granite ages (determined by U-Pb zircon LA-ICP-MS and multi-grain TIMS analyses) overlap at ca. 134 Ma. Two U-Pb multi-grain titanite dates, determined by TIMS, are consistent with the U-Pb zircon crystallization ages (Figs. 12g, h, 14). The tonalite is cut by the granite, and the results are best interpreted as concomitant metaluminous tonalitic and weakly peraluminous granitic magmatism, preserved as tonalite enclaves within granite intrusions (Figs. 4a, 12a-h). Four Mesilinka  $^{40}\text{Ar}/^{39}\text{Ar}$  biotite dates yield a range from  $123 \pm 2$  to  $108 \pm 2$  Ma (Figs.

13, 14). This is interpreted as a prolonged period of magmatic and post-deformation cooling following emplacement of the Mesilinka suite.

A fundamental geochemical subdivision of Hogem batholith exists between the silica-saturated Thane Creek, Osilinka, and Mesilinka suites and the mildly silica undersaturated Duckling Creek suite (0-12 wt.% normative nepheline). Despite their overlapping  $\text{SiO}_2$  concentrations, the diorites, quartz monzodiorites, and granodiorites of the Thane Creek suite ( $\text{SiO}_2=47-71$  wt.%) have significantly lower total alkali metal concentrations ( $\text{Na}_2\text{O}+\text{K}_2\text{O}=3.4-8.2$  wt.%) than the syenites of the Duckling Creek suite ( $\text{SiO}_2=53-64$  wt.%;  $\text{Na}_2\text{O}+\text{K}_2\text{O}=8.6-14.8$  wt.%). The higher  $\text{SiO}_2$  concentrations of the Mesilinka (63-77 wt.%) and Osilinka (69-76 wt.%) suites are reflected in higher relative abundances of modal quartz, although variable  $\text{K}_2\text{O}+\text{Na}_2\text{O}$  concentrations and  $\text{CaO}/(\text{Na}_2\text{O}+\text{K}_2\text{O})$  ratios result in a large compositional range between tonalite and syenogranite. Whereas the intermediate- $\text{SiO}_2$  rocks of the Thane Creek and Duckling Creek suites are metaluminous (Fig. 4a), the high- $\text{SiO}_2$  Mesilinka and Osilinka suites are weakly peraluminous ( $\text{ASI} \leq 1.2$ ) and similar to the estimated ASI of the upper continental crust (1.04; Rudnick and Gao, 2003). Samples of the Thane Creek suite are magnesian (Fig. 4b) according to the classification of Frost and Frost (2008), and clearly distinguished from the ferroan Duckling Creek

suite syenites. Although most of the samples of the Mesilinka suite are magnesian, a subset of the syenogranitic samples are ferroan and more similar to the syenogranite of the Osilinka suite (Fig. 4b). However, the two ferroan syenogranite suites are distinguished on their molar  $K/(K+Na)$  ratios; the ferrous syenogranites of the Mesilinka suite ( $K/(K+Na)=0.32-0.46$ ) are potassic relative to both the syenogranites of the Osilinka suite ( $K/(K+Na)=0.21-0.32$ ) and continental crust estimates ( $K/(K+Na) < 0.36$ ; Rudnick and Gao, 2003). In addition to the ferroan syenogranites of the Mesilinka suite, syenites of the Duckling Creek suites are also potassic ( $K/(K+Na)=0.32-0.68$ ). The remaining rocks of the Hagem batholith are relatively sodic and comparable to the continental crust composition.

The Hagem batholith contains chemically diverse igneous suites that have a punctuated and protracted intrusive history, lasting more than 80 m.y. This longevity is rare for a single batholith in the Canadian Cordillera and indicates that diverse magma sources were tapped through time. Further petrogenetic studies will help determine how each of the intrusive suites fit within the tectonic evolution of the orogen. A new finding in this study is that the Mesilinka suite (135-128 Ma) intruded during a previously documented magmatic gap in the Cordilleran orogen (Armstrong, 1988).

## 6. Economic implications

Both the Thane Creek and Duckling Creek suites host porphyry Cu-Au mineralization. The best example is the Lorraine deposit, which is hosted by Duckling Creek suite. It has an Indicated resource of 6.42 Mt at 0.62% Cu and 0.23 g/t Au and an Inferred resource of 28.82 Mt at 0.45% Cu and 0.19 g/t Au (Giroux and Lindinger, 2012). The Lorraine deposit is south of the present study area (Fig. 2; e.g., Devine et al., 2014), but equally prospective rocks are in northern Hagem batholith, as confirmed by our bedrock mapping and geochronological results (Figs. 2, 14; Ootes et al., 2020a, b, c). The Thane Creek suite hosts numerous Cu-prospects, some of which are actively being explored (e.g., Cathedral project, Naas, 2016; Top Cat, Serengeti Resources Inc., 2020), and correlative rocks host the Kwanika developed prospect south of the present study area (Serengeti Resources Inc., 2020). The results of this study confirm a similar age-relationship to the Cu-hosted Rhonda-Dorothy prospect to the south (Devine et al., 2014) and further highlight the distribution of the Thane Creek suite in Hagem batholith.

## Acknowledgments

The first author acknowledges support from the Diamond Exploration Research Training School (DERTS), which is funded by NSERC and the University of Alberta. The first author received additional funding from NSERC CGS-M and Geoscience BC. This is NRCan contribution 20200583. Reviews by F. Devine and J. Chiarenzelli helped improve the manuscript.

## References cited

- Armstrong, J.E., 1946. Aiken Lake (south half), British Columbia. Geological Survey of Canada, Paper 46-11, 1 sheet, scale 1 inch:2 miles.
- Armstrong, R.E., 1988. Mesozoic and early Cenozoic magmatic evolution of the Canadian Cordillera. In: Clark, S.P., Burchfiel, B.C., Suppe, J., (Eds.), Processes in Continental Lithospheric Deformation. Geological Society of America, Special Paper 218, pp. 55-90. <https://doi.org/10.1130/SPE218-p55>.
- Armstrong, J.E., and Roots, E.F., 1948. Aiken Lake map-area, British Columbia. Geological Survey of Canada, Paper 48-5, 46 p.
- Armstrong, J.E., and Roots, E.F., 1954. Aiken Lake, Cassiar District, British Columbia. Geological Survey of Canada, A Series Map 1030A, scale 1 inch:4 miles.
- Bath, A.B., Cooke, D.R., Friedman, R.M., Faure, K., Kamenetsky, V.S., Tosdal, R.M., and Berry, R.F., 2014. Mineralization, U-Pb geochronology, stable isotope geochemistry of the Lower Main Zone of the Lorraine deposit, north-central British Columbia: A replacement-style alkalic Cu-Au porphyry. *Economic Geology*, 109, 979-1004.
- CGG Canada Services Ltd., 2018. Geophysical survey report MIDAS high resolution magnetic and radiometric survey Search Project Phase III; Geoscience BC, Report 2018-2, 72 p.
- Devine, F.A.M., Chamberlain, C.M., Davies, A.G.S., Friedman, R., and Baxter, P., 2014. Geology and district-scale setting of tilted alkalic porphyry Cu-Au mineralization at the Lorraine deposit, British Columbia. *Economic Geology*, 109, 939-977.
- Ferri, F., Dudka, S.F., Rees, C., and Meldrum, D., 2001a. Geology of the Aiken Lake area, north-central British Columbia, NTS 94C/5, 6 and 12. British Columbia Ministry of Energy, Mines and Petroleum Resources, British Columbia Geological Survey Geoscience Map 2001-10, scale 1:50,000.
- Ferri, F., Dudka, S.F., Rees, C.J., Meldrum, D.G., and Willson, M.J., 2001b. Geology of the Uslika Lake Area, North-Central B.C. (NTS 94C/2, 3 & 4). British Columbia Ministry of Energy, Mines and Petroleum Resources, British Columbia Geological Survey Geoscience Map 2001-04, scale 1:50,000.
- Fisher, C.M., Vervoort, J.D., and Hanchar, J. M., 2014. Guidelines for reporting zircon Hf isotopic data by LA-MC-ICPMS and potential pitfalls in the interpretation of these data. *Chemical Geology*, 363, 125-133.
- Fisher, C.M., Paton, C., Pearson, D.G., Sarkar, C., Luo, Y., Tersmette, D.B., and Chacko, T., 2017. Data reduction of Laser Ablation Split-Stream (LASS) analyses using newly developed features within Iolite: With applications to Lu-Hf+ U-Pb in detrital zircon and Sm-Nd+ U-Pb in igneous monazite. *Geochemistry, Geophysics, Geosystems*, 18, 4604-4622.
- Flowers, R.M., Bowring, S.A., Tulloch, A.J., and Klepeis, K.A., 2005. Tempo of burial and exhumation within the deep roots of a magmatic arc, Fiordland, New Zealand. *Geology*, 33, 17-20.
- Frost, B.R., and Frost, C.D., 2008. A geochemical classification for feldspathic igneous rocks. *Journal of Petrology* 49, 1955-1969.
- Garnett, J.A., 1972. Preliminary geological map of part of Hagem batholith, Duckling Creek area (parts of NTS 93N/13, 14; 94C/3, 4). British Columbia Ministry of Energy, Mines and Petroleum Resources, British Columbia Geological Survey Preliminary Map 09, scale 1:50,000.
- Garnett, J.A., 1978. Geology and mineral occurrences of the southern Hagem batholith. British Columbia Ministry of Energy, Mines and Petroleum Resources, British Columbia Geological Survey Bulletin 70, 75 p.
- Giroux, G., and Lindinger, L.J., 2012. Summary report on the Lorraine-Jajay property, Omenica Mining Division, B.C. Prepared for Lorraine Copper Corp., Report 09-2012, 122 p., URL <[http://www.sedar.com/issuers/issuers\\_en.htm](http://www.sedar.com/issuers/issuers_en.htm)>, last accessed October, 2020.

- Irvine, T.N., 1976. Studies of Cordilleran gabbroic and ultramafic intrusions, British Columbia. Geological Survey of Canada, Paper 76-1A, pp. 75-81.
- Jones, G.O., Pearson, D.G., Vezinet, A., Luo, Y., Stern, R.A., Milidragovic, D., and Ootes, L., 2021. Preliminary zircon geochemistry of northern Hogem batholith, Quesnel terrane, north-central British Columbia (parts of NTS 093M/16, 093N/13, 14, 094C/03-06, 094D/01, 08). Geoscience BC Summary of Activities 2020: Minerals and Mining, Report 2021-1, in press.
- Kuiper, K.F., Deino, A., Hilgen, F.J., Krijgsman, W., Renne, R., and Wijbrans, J.R., 2008. Synchronizing rock clocks of Earth history. *Science*, 320, 500-504.
- Le Maitre, R., Streckeisen, A., Zanettin, B., Le Bas, M., Bonin, B., and Bateman, P., (Eds.), 2002. *Igneous Rocks: A Classification and Glossary of Terms: Recommendations of the International Union of Geological Sciences Subcommittee on the Systematics of Igneous Rocks*. Cambridge: Cambridge University Press.
- Lord, C.S., 1948. McConnell Creek map-area, Cassiar District, British Columbia. Geological Survey of Canada, Memoir 251, 82 p.
- Lord, C.S., 1949. McConnell Creek, Cassiar District, British Columbia. Geological Survey of Canada, A Series Map 962A, scale 1 inch:4 miles.
- Ludwig, K.R., 2003. *Isoplot 3.00: A geochronological toolkit for Microsoft Excel*. Berkeley Geochronology Center, Berkeley, 70 p.
- Mortensen, J.K., Ghosh, D.K., and Ferri, F., 1995. U-Pb geochronology of intrusive rocks associated with copper-gold porphyry deposits in the Canadian Cordillera. *Canadian Institute of Mining, Metallurgy and Petroleum, Special Volume 46*, pp. 142-158.
- Naas, C.O., 2016. Lidar surveying, ground magnetic surveying and geochemical sampling of the Cathedral property. British Columbia Geological Survey, Assessment Report 36337, 151 p.
- Nelson, J.L., Colpron, M., and Israel, S., 2013. The Cordillera of British Columbia, Yukon, and Alaska: Tectonics and metallogeny. In: Colpron, M., Bissing, T., Rusk, B.G., and Thompson, J.F.H., (Eds.), *Tectonics, Metallogeny, and Discovery: The North American Cordillera and similar accretionary settings*. Society of Economic Geologists, Special Publication 17, pp. 53-109.
- Nixon, G.T., and Peatfield, G.R., 2003. Geological setting of the Lorraine Cu-Au porphyry deposit, Duckling Creek syenite complex, north-central British Columbia. British Columbia Ministry of Energy and Mines, British Columbia Geological Survey Open File 2003-4, 24 p.
- Ootes, L., Bergen, A., Milidragovic, D., Graham, B., and Simmonds, R., 2019. Preliminary geology of northern Hogem batholith, Quesnel terrane, north-central British Columbia. In: *Geological Fieldwork 2018*, British Columbia Ministry of Energy, Mines and Petroleum Resources, British Columbia Geological Survey Paper 2019-01, pp. 31-53.
- Ootes, L., Bergen, A.L., Milidragovic, D., and Jones, G.O., 2020a. Preliminary geology of the northern Hogem batholith and its surroundings, north-central British Columbia. British Columbia Ministry of Energy and Mines and Petroleum Resources, British Columbia Geological Survey Open File 2020-02, scale 1:50,000.
- Ootes, L., Bergen, A.L., Milidragovic, D., Jones, G.O., Camacho, A., and Friedman, R., 2020b. An update on the geology of northern Hogem batholith and its surroundings, north-central British Columbia. In: *Geological Fieldwork 2019*, British Columbia Ministry of Energy, Mines and Petroleum Resources British Columbia Geological Survey Paper 2020-1, pp. 25-47.
- Ootes, L., Jones, G.O., Schiarizza, P., Milidragovic, D., Friedman, R., Camacho, A., Luo, Y., Vezinet, A., Pearson, D.G., and Zhang, S., 2020c. Geochronologic and geochemical data from northern Hogem batholith and its surroundings, north-central British Columbia. British Columbia Ministry of Energy and Mines Low Carbon Innovation, British Columbia Geological Survey GeoFile 2020-01, 21 p.
- Paton, C., Hellstrom, J., Paul, B., Woodhead, J., and Hergt, J., 2011. *Iolite: Freeware for the visualization and processing of mass spectrometric data*. *Journal of Analytical Atomic Spectrometry*, 26, 2508-2518.
- Paton, C., Woodhead, J.D., Hellstrom, J.C., Hergt, J.M., Greig, A., and Maas, R., 2010. Improved laser ablation U-Pb zircon geochronology through robust downhole fractionation correction. *Geochemistry, Geophysics, Geosystems*, 11, <https://doi.org/10.1029/2009GC002618>.
- Roots, E.F., 1954. Geology and mineral deposits of Aiken Lake map area, British Columbia. Geological Survey of Canada, Memoir 274, 246 p.
- Rudnick, R.L., and Gao, S., 2003. Composition of the Continental Crust. In: *The Crust*, Rudnick, R.L., (Ed.), *Treatise on Geochemistry* 3, pp. 1-64.
- Schiarizza, P., and Tan, S.H., 2005a. Geology and mineral occurrences of the Quesnel Terrane between the Mesilinka River and Wrede Creek (NTS 94D/8, 9), north-central British Columbia. British Columbia Ministry of Energy and Mines, British Columbia Geological Survey Paper 2005-1, pp. 109-130.
- Schiarizza, P., and Tan, S.H., 2005b. Geology of the Johanson Lake area, parts of NTS 94D/8 and 9. British Columbia Ministry of Energy, Mines and Petroleum Resources, British Columbia Geological Survey Open File 2005-4, scale 1:50,000.
- Schmitz, M.D., and Schoene, B., 2007. Derivation of isotope ratios, errors, and error correlations for U-Pb geochronology using  $^{205}\text{Pb}$ - $^{235}\text{U}$ -( $^{233}\text{U}$ )-spiked isotope dilution thermal ionization mass spectrometric data. *Geochemistry, Geophysics, Geosystems*, 8, <https://doi.org/10.1029/2006GC001492>.
- Serengeti Resources Inc., 2020. Projects overview. <https://www.serengetiresources.com/projects/projects-overview-1>, last accessed October, 2020.
- Shand, S.J., 1943. *Eruptive Rocks; Their Genesis, Composition, Classification, and Their Relation to Ore Deposits, with a Chapter on Meteorites (Revised Second Edition)*. Hafner Publishing Co., New York.
- Stanley, C., 2017. Lithochemical classification of igneous rocks using Streckeisen ternary diagrams. *Geochemistry: Exploration, Environment, Analysis*, 17, 63-91.
- Vermeesch, P., 2018. *IsoplotR: A free and open toolbox for geochronology*. *Geoscience Frontiers*, 9, 1479-1493.
- Vezinet, A., Pearson, D.G., Thomassot, E., Stern, R.A., Sarkar, C., Luo, Y., and Fisher, C.M., 2018. Electronic Supplementary Material: Hydrothermally-altered mafic crust as source for early Earth TTG: Pb/Hf/O isotope and trace element evidence from TTG of the Eoarchean Saglek Block, N. Labrador. *Earth and Planetary Science Letters*, 503, 95-107.
- Woodsworth, G.J., 1976. Plutonic rocks of McConnell Creek (94 D west half) and Aiken Lake (94 C east half) map-areas, British Columbia. Geological Survey of Canada, Paper 76-1A, pp. 69-73.